Transitions between NiAs and MnP Type Phases: An Electronically Driven Distortion of Triangular (3^6) Nets

Wolfgang Tremel,[1] Roald Hoffmann,* and Jérôme Silvestre

Contribution from the Department of Chemistry and Materials Science Center, Cornell University, Ithaca, New York 14853. *Received October 3, 1985*

Abstract: An interesting sequence of deformations from the NiAs structure type occurs in simple 3d transition-metal phosphides. Whereas for d^1 and d^2 electron counts the NiAs structure type is preferred, for d^3 to d^6 electron counts a distortion to the MnP type structure occurs, breaking the triangular (3^6) nets of atoms and involving the formation of metal–metal and phosphorus–phosphorus zigzag chains. Going to a d^7 electron count we find a double pairing distortion in the NiP structure with metal and phosphorus pairs. The first deformation is driven by a second-order Jahn–Teller-like distortion, splitting a strong peak in the density of states of the NiAs structure. The distortion from the MnP to the NiP structure type is traced to bond formation between pairs of metal and phosphorus atoms, the driving force being the introduction of an energy gap close to the Fermi level.

The hexagonal NiAs structure is one of the most common AB structures in transition-metal chemistry. It has a unique position in crystal chemistry, being intermediate between predominantly ionic compounds with a NaCl structure and intermetallic compounds having the CsCl structure.[2] Over 100 compounds crystallize with the NiAs or related structures, and with very few exceptions all contain transition-metal atoms in combination with metalloid or B-group atoms.[3] The more metallic phases have many properties characteristic of intermetallic phases: opacity, metallic lustre, and conductivity. The great variety of electrical and magnetic properties originating from the variable composition makes them interesting materials in metallurgy.

On the other hand, in crystal chemistry the NiAs structure is of fundamental importance in ordering the wealth of known structures and in helping to elucidate structural principles. The graphical connection of topologically related structures can be represented as a hierarchic ordering in the form of a family tree,[4] the NiAs structure as a high symmetry parent structure being a so-called aristotype.[5] In the NiAs lattice, shown in **1**, the metal atoms A occupy the corners of a primitive hexagonal cell. In each cell one B atom is situated in the center of a hexagonal prism formed by six A atoms. There are two possibilities to build in

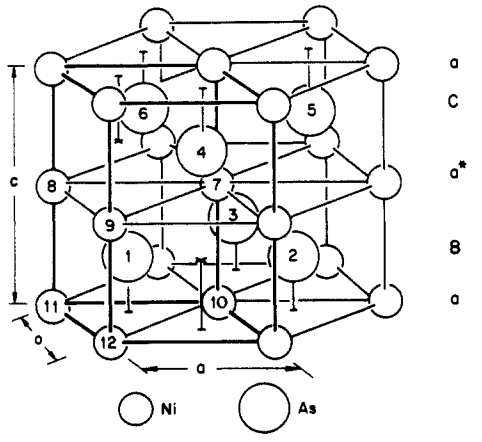

1

the B atoms, which are realized in an alternative manner in the *c*-direction. The result is a doubling of the repeat unit in the direction of the hexagonal *c*-axis. To put it more concisely, in the NiAs structure the group B atoms form a hexagonal close-packed sublattice, which is interpenetrated by a primitive hexagonal sublattice of metal atoms. The stacking sequence of these triangular nets (or 3^6 nets in the Schläfli notation) is a C a B a.... Metal atoms occupy octahedral and group B atoms trigonal prismatic voids. The resulting coordination is 6:6, but since the Ni coordination octahedra are stacked in columns where each octahedron shares a pair of opposite faces with adjacent octahedra, there are also two short metal–metal contacts. For ideal close packing the axial ratio c/a is $\sqrt{8/3} = 1.633$. NiAs phases extend over a considerable range of composition; what is changing in the process is only the c/a ratio.

The importance of the NiAs structure ($B8_1$)[6] in crystal chemistry is that other common structure types can easily be generated by certain pathways of symmetry reduction. Taking away every second layer of metal atoms gives the composition $A_{0.5}B$, which is found in the well-known layered structure of CdI_2; filling the empty trigonal prismatic sites in **1** would lead to the composition A_2B as found in the case of the anti-AlB_2 or Ni_2In structure.[7] Other modifications are changes in the stacking sequence as in the TiP structure **2**.[8] Here every second layer of nonmetal atoms is not trigonal prismatically, but octahedrally coordinated. This results in an alternating layer sequence similar to those found in the NiAs and anti-CdI_2 structure. In other words, the TiP structure may be regarded as an hc close packing of P-atoms with metal atoms in the octahedral voids.

One of the most common derivatives of the NiAs structure is the orthorhombic ($B31$)[6] MnP structure[9] met among the pnictides.[10] In this structure the hexagonal symmetry is broken and the most convenient starting point to explain this structure is by transforming the primitive hexagonal NiAs-cell into a C-centered orthorhombic cell. Next the cations are displaced in the plane

(1) DAAD/NATO Postdoctoral Fellow 1984–1985.
(2) Cornish, A. J. *Acta Metall.* **1958**, *6*, 371.
(3) For reviews see: Kjekshus, A.; Pearson, W. B. *Prog. Solid State Chem.* **1964**, *1*, 83. Hulliger, F. *Struct. Bonding (Berlin)* **1968**, *4*, 83.
(4) Bärnighausen, H. *Commun. Math. Chem.* **1980**, *9*, 1.
(5) Megaw, H. D. *Crystal Structures: A Working Approach*; Saunders Co.: Philadelphia, **1973**; p 282.
(6) Strukturbericht symbols like $B8_1$ are an alternative way to indicate structure types. For a listing of structure types see: Pearson, W. B. *A Handbook of Lattice Spacings and Structures of Metals and Alloys*; Pergamon Press: Oxford, 1958; Vol. I.
(7) Wells, A. F. *Structural Inorganic Chemistry*, 4th ed.; Clarendon Press: Oxford, 1975. Krebs, H. *Grundzüge des Anorganischen Kristallchemie*, Ferdinand Enke Verlag: Stuttgart, 1968.
(8) Schönberg, N. *Acta Chem. Scand.* **1954**, *8*, 1460.
(9) (a) Rundqvist, S. *Acta Chem. Scand.* **1962**, *16*, 287. (b) Rundqvist, S.; Nawapong, P. C. *Acta Chem. Scand.* **1965**, *19*, 1006.
(10) For reviews see: (a) Rundqvist, S. *Ark. Kemi* **1962**, *20*, 67. (b) Lundström, T. *Ark. Kemi* **1969**, *31*, 227.

0002-7863/86/1508-5174$01.50/0 © 1986 American Chemical Society

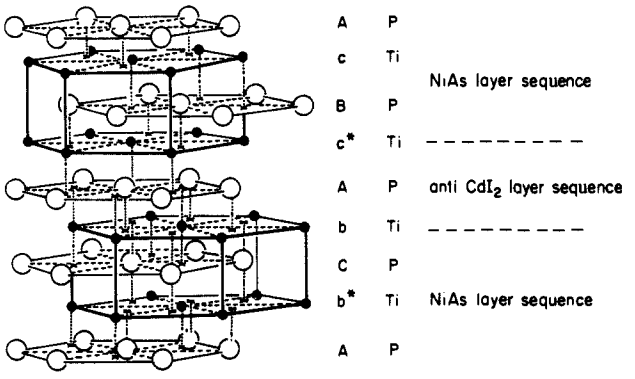

2

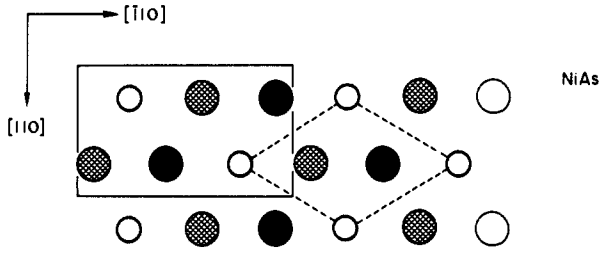

3

normal to the hexagonal axis, and the anions are shifted along this axis, as shown in **4** and **5** in a top view. Whereas in the NiAs

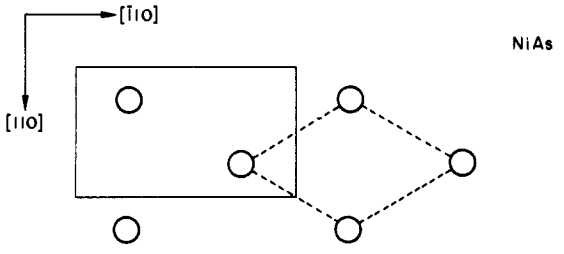

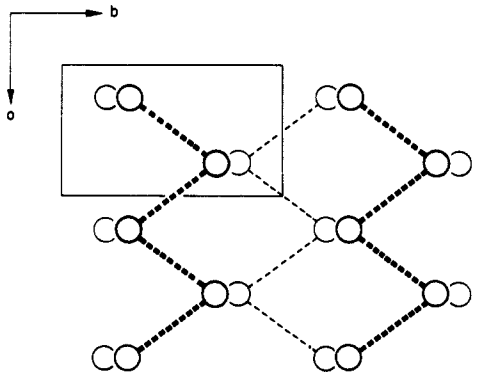

4

structure each cation has two close metal–metal contacts, it has another two at somewhat larger distances in the MnP-structure **6**. We find zigzag chains of metal atoms running in the *c*-direction,[11] and chains of metal and of phosphorus atoms running in the *a*-direction are formed by the distortion. The newly formed metal–metal and phosphorus–phosphorus contacts are 2.81 and 2.66 Å, respectively, in the MnP structure. From another point

(11) The standard space group setting for the MnP structure is *Pnma* (No. 62).[12] To be consistent with the choice of axes in the hexagonal system, we chose the nonstandard setting *Pmcn*.

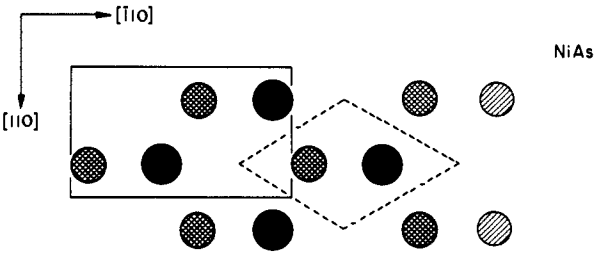

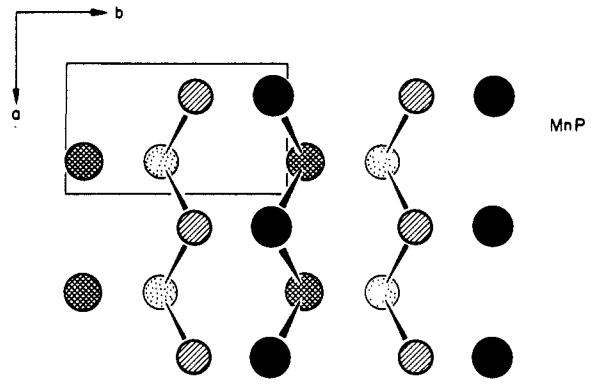

5

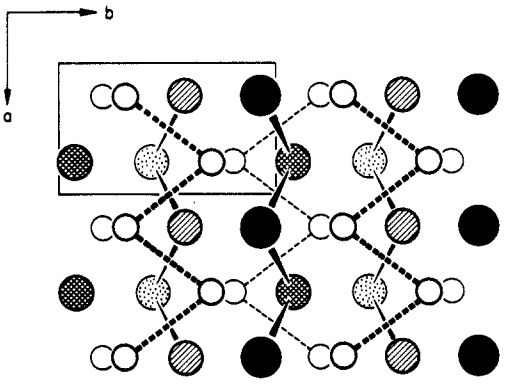

6

of view the deformation may be described as a *distortion of triangular* (3^6) *nets of atoms* to form a zigzag chain pattern. The two steps we just carried out can be put on a more formal basis by using the notation[4] of **7** (see Appendix II for explanation). The

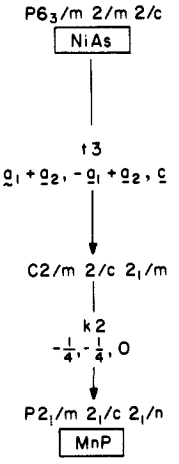

7

new choice of axis is the C-centered orthorhombic cell. As shown

in 7, it changes the point but not the translational symmetry; all symmetry elements connected with the sixfold axis except $C_{2z}|\vec{c}/2^* = C_{6z}^3|\vec{c}/2^*$ are lost. The first step is called "translationsgleich" for this reason. In the second stage the C-centering due to the intermediate space group *Cmcm* is lost in the actual distortion step. If we stay in the orthorhombic system, the point symmetry is still the same as for the intermediate structure. What is happening is a dilution of symmetry elements as translational symmetry is lost. Therefore this step is called "klassengleich".[12-14] The origin of the hexagonal cell has to be shifted by $^1/_4$, $^1/_4$, 0 (indicated in 7), and the standard setting *Pnma* can be achieved from *Pmcn* by cyclic permutation of the lattice constants.

The existence of the group–subgroup relations in **8** allows a continuous displacive transition between NiAs and MnP type structures.[15] In fact, this transition occurs for a number of compounds[16] and has been investigated by solid-state chemists/physicists for a long time.[17] Most of the interest stems from the peculiar structural and magnetic transitions, which some materials like $Mn_{1-t}T_tP$ (T = transition metal) undergo with changes in temperature, pressure, composition, and magnetic field.[18]

There are still further variants of the MnP structure. In the orthorhombic NiP structure,[19] **9**, metal chains are in the *xy* (paper) plane and the phosphorus chains have been transformed into pairs. The P–P distance within one pair is 2.43 Å, only slightly longer than a normal P–P single bond, e.g., the P–P bond length of 2.21 Å in the P_4-molecule.[20] The way the distortion occurs is by moving the metal atoms in the *a*-direction,[21] off the mirror plane which is still present in the MnP-type structure. In addition, however, in every second "layer" the metal atoms shift along *b*; so in the top view of **8** two metal atoms switch places compared to the projection of the MnP-type structure **6**. This motion produces a nonsymmorphic symmetry element in the *a*-direction, in that it connects two atoms by a twofold screw axis instead of a simple translation. The result is a doubling of the unit cell *a*-axis with respect to the MnP structure type. The coordination around each Ni-atom is modified by the distortion as the Ni-atoms move toward a corner of the distorted anion octahedron, leaving Ni in an effective 5-coordinate environment.

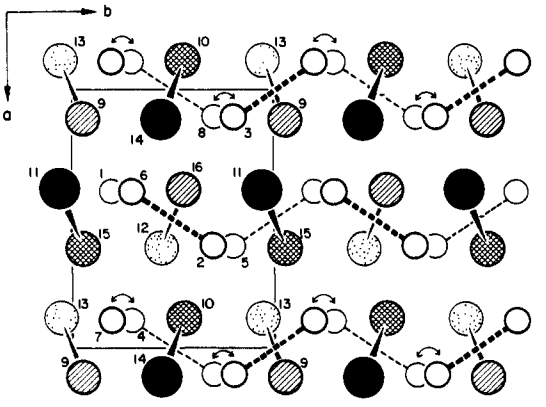

8

For the phosphides the occurrence of a given structure can be related to the electron count. In Table I the phosphides are arranged according to the number of valence electrons per formula unit. For 10 and fewer electrons the NiAs type structure (or a stacking variant) is found. For more than 14 electrons/unit cell the NiP structure is preferred. The stability maximum of the MnP-type structure is for electron counts ranging from 11 to 14 per unit cell, or in other words from d^2 to d^6 systems.

For the arsenides this trend is diluted; many compounds show both structure types, and for the stibnides, where metal and Sb bands overlap substantially, the NiAs structure is almost the only one encountered.

The careful reader may wonder why the electron counting scheme in Table I is not extended to other compounds such as transition-metal sulfides. For the 4d and 5d metals almost no stoichiometric monochalcogenides have been made. For the 3d metal sulfides, however, a similar trend as for the phosphides has been observed, although less pronounced. TiS and CrS, for instance, crystallize in the NiAs structure.[27a,b] Stoichiometric VS crystallizes in the MnP structure,[17] but it undergoes a continuous displacive phase transition to the NiAs structure at ≅550 °C. This phase transition has been investigated particularly well because of its second-order nature.[17] For FeS, CoS, and NiS the high-temperature form occurs in the NiAs structure,[27d,f] MnS—an exception in this series—is a magnetic semiconductor in the NaCl or ZnS structure.[27c] The fact that the "switch" from NiAs to MnP structure can be observed for the sulfides as well (although magnetic interactions may play a role in determining the structure) gives us some confidence that our approach is quite generally valid and not that it just happens to work out for the phosphides.

We would like to understand the origin of the observed distortions, for instance why MnP prefers its structure to the high-symmetry NiAs and the very distorted NiP structure type. A number of different explanations of the NiAs–MnP distortion have been proposed before. In VS the analogous transition has been ascribed to a charge density wave mechanism.[28a-c] Haas[28d-f] discussed the distortion pattern in terms of a model with isotropic

(12) *International Tables for Crystallography*; Hahn, T., Ed.; D. Reidel Publishing Co.: Dordrecht (Holland), Boston (USA), 1983; Vol. A.
(13) Neubüser, J.; Wondratschek, H. *Krist. Tech.* **1966**, *1*, 529.
(14) Burzlaff, H.; Zimmermann, H. *Kristallographie: Grundlagen und Anwendungen*; Bd. 1; Thieme Verlag: Stuttgart, 1977.
(15) (a) Franzen, H. F. *Second Order Phase Transitions and the Irreducible Representations of Space Groups*; Springer-Verlag: Berlin, Heidelberg, New York, 1982; Lecture Notes in Chemistry, Vol. 32. (b) Franzen, H. F.; Haas, C.; Jellinek, F. *Phys. Rev.* **1974**, *B10*, 1248. (c) Bertaut, E. F. *C. R. Acad. Sci. Sci., Ser. 2* **1982**, *295*, 539. (d) Aizu, K. *J. Phys. Soc. Jpn.* **1969**, *27*, 387.
(16) (a) $Mn_{0.9}Fe_{0.1}As$: Selte, K.; Kjekshus, A. *Acta Chem. Scand.* **1973**, *27*, 3607. (b) $Mn_{0.9}Fe_{0.1}As_1$, CrAs, CoAs: Selte, K.; Kjekshus, A. *Acta Chem. Scand.* **1973**, *27*, 3195. (c) $Mn_{1-t}Mo_tAs$: Fjellvåg, H.; Selte, K.; Danihelka, P. *Acta Chem. Scand.* **1984**, *A38*, 789. (d) $Cr_{1-t}Fe_tAs$: Selte, K.; Fjellvåg, H.; Kjekshus, A.; Andresen, A. F. *Acta Chem. Scand.* **1979**, *A33*, 727.
(17) (a) Franzen, H. F.; Burger, T. J. *J. Chem. Phys.* **1968**, *49*, 2268. (b) Franzen, H. F.; Strachnan, D. M.; Barnes, R. G. *J. Solid State Chem.* **1973**, *7*, 374. (c) Franzen, H. F.; Wiegers, G. A. *J. Solid State Chem.* **1975**, *13*, 114. (d) Franzen, H. F.; Sawatzky, G. A. *J. Solid State Chem.* **1975**, *15*, 229. (e) Franzen, H. F.; Leebrick, D. H.; Laabs, F. *J. Solid State Chem.* **1975**, *13*, 307. (f) Nakahara, J.; Franzen, H. F.; Misemer, D. K. *J. Chem. Phys.* **1982**, *76*, 4080. (g) Silvestre, J.; Tremel, W.; Hoffmann, R. *J. Less-Common Met.* **1986**, *116*, 113.
(18) (a) Selte, K.; Brikeland, L.; Kjekshus, A. *Acta Chem. Scand.* **1978**, *A32*, 731. (b) Selte, K.; Fjellvåg, H.; Kjekshus, A. *Acta Chem. Scand.* **1979**, *A33*, 391. (c) Fjellvåg, H.; Kjekshus, A. *Acta Chem. Scand.* **1984**, *A38*, 563. (d) Fjellvåg, H.; Kjekshus, A. *Acta Chem. Scand.* **1984**, *A38*, 703. (e) Fjellvåg, H.; Kjekshus, A.; Andresen, A. F. *Acta Chem. Scand.* **1984**, *A38*, 711. (f) Fjellvåg, H.; Kjekshus, A. *Acta Chem. Scand.* **1984**, *A38*, 719. (g) Fjellvåg, H.; Kjekshus, A.; Andresen, A. F. *Acta Chem. Scand.* **1985**, *A39*, 143. (h) Fjellvåg, H.; Kjekshus, A. *Acta Chem. Scand.* **1985**, *A39*, 199. (i) Fjellvåg, H.; Kjekshus, A. *Acta Chem. Scand.* **1986**, *A40*, 8. (j) Podloucky, R. *J. Magn. Magn. Mat.* **1984**, *43*, 204, 291.
(19) Larsen, E. *Ark. Kemi* **1964**, *23*, 335.
(20) Maxwell, L. R.; Henricks, S. B.; Mosley, V. M. *J. Chem. Phys.* **1935** *3*, 699.
(21) The setting chosen is not the standard setting, although the space group is still *Pbca*.
(22) Irani, K. S.; Gingerich, K. A. *J. Phys. Chem. Solids* **1963**, *24*, 1153.
(23) Jeitschko, W.; Nowotny, H. *Monatsh. Chem.* **1962**, *93*, 1107, 1284.
(24) Boller, H.; Parthé, E. *Acta Crystallogr.* **1963**, *16*, 1095.
(25) Rundqvist, S.; Lundström, T. *Acta Chem. Scand.* **1963**, *17*, 37.
(26) Raub, C. J.; Zachariasen, W. H.; Geballe, G. H.; Matthias, B. T. *J. Phys. Chem. Solids* **1963**, *24*, 1093.
(27) (a) TiS: Hahn, H.; Harder, B. *Z. Anorg. Allg. Chem.* **1956**, *288*, 241. (b) CrS: Kamigaichi, T.; Masumoto, K.; Hihara, T. *J. Phys. Soc. Jpn.* **1960**, *15*, 1355. (c) MnS: Corliss, L.; Elliott, N.; Hastings, J. *Phys. Rev.* **1956**, *104*, 924. Rooymans, C. J. M. *J. Inorg. Nucl. Chem.* **1963**, *25*, 253. (d) Andresen, A. F. *Acta Chem. Scand.* **1960**, *14*, 919. (e) CoS: *Strukturbericht* **1931**, *1*, 84. (f) NiS: Trahan, J.; Goodrich, R. G.; Watkins, S. T. *Phys. Rev. B* **1970**, *2*, 2858. McWhan, D. B.; Marezio, M.; Remeika, J. P.; Dernier, P. D. *Ibid.* **1972**, *5*, 2552.
(28) (a) Liu, S. H. *Phys. Rev.* 1974, *B10*, 3619. (b) Liu, S. H.; England, W. B.; Myron, H. W. *Solid State Commun.* **1974**, *14*, 1003. (c) England, W. B.; Liu, S. H.; Myron, H. W. *J. Chem. Phys.* **1974**, *60*, 3760. (d) Haas, C. *Solid State Commun.* **1978**, *26*, 709. (e) van Bruggen, C. F.; Haas, C.; Wiegers, G. A. *J. Solid State Chem.* **1979**, *27*, 9. (f) Haas, C. *J. Solid State Chem.* **1985**, *57*, 82.

Table I. Distribution of the Phosphide Structure Types as a Function of the Electron Count per Formula Unit

structure type	no. of valence electrons						
	9	10	11	12	13	14	15
NiAs	TiP	VP					
	ZrP[a]	NbP[c]					
	HfP[b]	TaP[c]					
MnP			CrP[d]	MnP	FeP[d]	CoP[d]	
			MoP[e]		RuP[g]		
			WP[f]			IrP[h]	
NiP							NiP

[a] TiP structure, ref 22. [b] TiP structure, ref 23. [c] Transposition structure of WC type, ref 24. [d] Reference 8. [e] WC-type, ref 24. [f] Reference 24. [g] Reference 25. [h] Reference 26.

attractive interactions between atoms placed on a hexagonal lattice. If only nearest-neighbor interactions are considered, the MnP structure is one of two stable distorted structures. This would account for the widespread occurrence of this zigzag chain type distortion in other compounds such as $MoTe_2$, $NbTe_2$ and $TaTe_2$,[2b,15,29] ZrI_2,[30] Nb_2Se_3,[31] Cr_3S_4,[32] Mo_2As_3[33] or Nb_3Se_4, and related[34] structures. We note here some important work done by Pettifor and Podloucky,[35] who explain the structural stability of AB compounds within a tight-binding model which allows influences of atomic size, atomic energy-level differences, and electron count to be examined in detail.

We will proceed in this paper by first building up the electronic structure for the NiAs type structure and then making the distortions to the MnP and NiP structures. Our calculations are of the extended Hückel type[36,37] in the tight-binding[38] approximation. Calculational details are listed in Appendix I. To simplify the analysis we use a rigid band model, doing the actual calculations on MnP in the NiAs, MnP, and NiP structures. Our calculations are nonmagnetic, i.e., they do not allow electrons of different spin to occupy different orbitals. This limitation imposes some restraints on our conclusions, and we will mention this point again.

Bonding in the NiAs Structure

The same fragmentation principles in terms of packing, coordination polyhedra or nets that apply to the geometrical description of solid-state structures can be used in analyzing their electronic structure as well. A pragmatic view is probably most effective. We can get an initial schematic picture of the bonding in the NiAs type lattice from a ligand field model. In the next step, in order to explain our calculated band structure, we will break up the NiAs type lattice into nonmetal and metal sublattices. This corresponds—as we shall see—to a fragmentation in terms of stacked triangular nets.

Let us start with the ligand field model, turning on the strongest Mn–P bonding first, in **9**. Some metal–P σ bonding orbitals, mainly on P, should go down; some metal–P σ antibonding orbitals, mainly on the metal, go up. The local environment at the metal is a slight trigonal distortion of octahedral, so one should see a typical three below two pattern in the d block. At this point the level scheme is no different from that of a typical octahedral transition metal complex, say $Mn(PR_3)_6$.

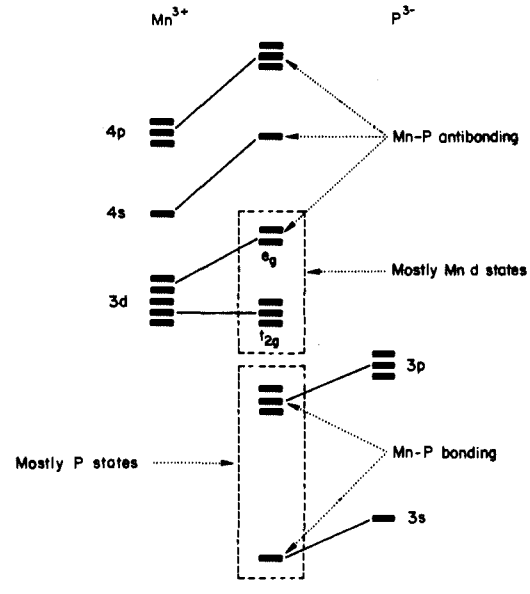

9

Now metal–metal interactions are turned on. These are not weak, and while they are stronger along the *c*-axis they really are three dimensional. The t_{2g} and e_g components would be expected to spread out into one band. The t_{2g} and e_g based bands would be expected to overlap, as would the two symmetry distinguished ($\Gamma_\parallel(z^2)$ and $\Gamma_\perp$) components of the t_{2g} origin bands. Nevertheless, we might hope for a rough correlation, based on the greater strength of axial bonding in which z^2 participates, along the lines of **10**.

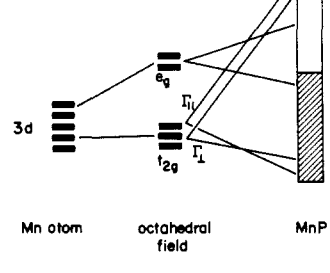

10

(29) Hulliger, F. In *Structural Chemistry of the Layer-Type Phases*; Levy, F., Ed.; Reidel: Dordrecht, 1976; p 247.
(30) Corbett, J. D.; Guthrie, D. H. *Inorg. Chem.* **1982**, *21*, 1247.
(31) Kadijk, F.; Huisman, R.; Jellinek, F. *Acta Crystallogr.* **1968**, *B24*, 1102. Mo_2S_3 has a slightly different structure, as recent results show: Debliek, R.; Wiegers, G. A.; Bronsema, K. D.; van Dyck, D.; Van Tendeloo, G.; Van Landuyt, J.; Amelinckx, S. *Phys. Status Solidi* **1983**, *A77*, 249. Compare to: De Jonge, R.; Popma, T. J. A.; Wiegers, G. A.; Jellinek, E. *J. Solid State Chem.* **1970**, *2*, 188.
(32) Jellinek, F. *Acta Crystallogr.* **1957**, *10*, 620.
(33) Jensen, P.; Kjekshus, A.; Skansen, T. *Acta Chem. Scand.* **1966**, *20*, 1003.
(34) (a) Nb_3S_4: Ruysink, A. F.; Kadijk, F.; Wagner, A. J.; Jellinek, F. *Acta Crystallogr.* **1968**, *B24*, 1614. (b) Nb_3Se_4, Nb_3Te_4: Selte, K.; Kjekshus, A. *Acta Crystallogr.* **1964**, *17*, 1568. (c) $Pb_{0.15}Nb_3S_4$: Amberger, E.; Polborn, K.; Grimm, P. *Acta Crystallogr.* **1985**, *C41*, 306. (d) $A_xNb_3S_4$: Schöllhorn, R.; Schramm, W. *Z. Naturforsch.* **1979**, *B34*, 697. (e) $Tl_xV_6S_8$: Vlasse, M.; Fournès, L. *Mater. Res. Bull.* **1976**, *11*, 1527. (f) $Tl_{0.76}Ti_6Se_8$, $Tl_{0.76}Nb_6Se_8$: Boller, H.; Klepp, K. *Mater. Res. Bull.* **1983**, *18*, 437. (g) $K_xTi_3S_4$: Schöllhorn, R.; Schramm, W.; Fenske, D. *Angew. Chem.* **1980**, *92*, 477; *Angew. Chem., Int. Ed. Engl.* **1980**, *19*, 492. (h) TlV_5S_8: Fournès, L.; Vlasse, M.; Saux, M. *Mater. Res. Bull.* **1977**, *12*, 1. (i) $Tl_xV_5S_8$: Schramm, W.; Schöllhorn, R.; Eckert, H.; Müller-Warmuth, W. *Mater. Res. Bull.* **1983**, *18*, 1283. (j) V_3Se_4: Kallel, A.; Boller, H. *J. Less-Common Met.* **1984**, *102*, 213. (k) TlV_5Se_8: Klepp, K.; Boller, H. *J. Solid State Chem.* **1983**, *48*, 388. Bensch, W.; Polborn, K.; Amberger, E.; Steurer, W.; Abart, J. *J. Solid State Chem.* **1984**, *55*, 121. (l) V_5S_8: Kawada, I.; Nakano-Onoda, M.; Ishii, M.; Saeki, M.; Nahahira, M. *J. Solid State Chem.* **1975**, *15*, 246. (m) $K_xV_5S_8$: Bronsema, K. D.; Jansen, R.; Wiegers, G. A. *Mater. Res. Bull.* **1984**, *19*, 555. (n) TlV_5S_8, TlV_6S_8: Ohtani, T.; Onoue, S. *Mater. Res. Bull.* **1986**, *21*, 69. (o) TlV_6S_8: Fournes, L.; Vlasse, M. *Rev. Chim. Miner.* **1978**, *15*, 542. (p) ACr_5S_8: Platte, C.; Sabrowsky, H. *Naturwissenschaften* **1975**, *62*, 528. Huster, J. *Z. Anorg. Allg. Chem.* **1978**, *447*, 89; *Z. Kristallogr.* **1979**, *149*, 146. For band structure calculations see: (q) Oshiyama, A. *Solid State Commun.* **1982**, *43*, 607. (r) Oshiyama, A. *J. Phys. Soc. Jpn.* **1983**, *52*, 587. (s) Bullett, D. W. *J. Solid State Chem.* **1980**, *33*, 13. (t) Canadell, E.; Whangbo, M.-H. *Inorg. Chem.* **1986**, *25*, 1488.
(35) Pettifor, D. G.; Podloucky, R. *Phys. Rev. Lett.* **1984**, *53*, 1080.
(36) Hoffmann, R. *J. Chem. Phys.* **1963**, *34*, 1397. Hoffmann, R.; Lipscomb, W. M. *Ibid.* **1962**, *36*, 3179, 3489; **1962**, *37*, 2872.
(37) Ammeter, J. H.; Bürgi, H.-B.; Thibeault, J. C.; Hoffmann, R. *J. Am. Chem. Soc.* **1978**, *100*, 3686.
(38) (a) Whangbo, M.-H.; Hoffmann, R. *J. Am. Chem. Soc.* **1978**, *100*, 6093. (b) Whangbo, M.-H.; Hoffmann, R.; Woodward, R. B. *Proc. R. Soc. London, Ser. A* **1979**, *366*, 23.

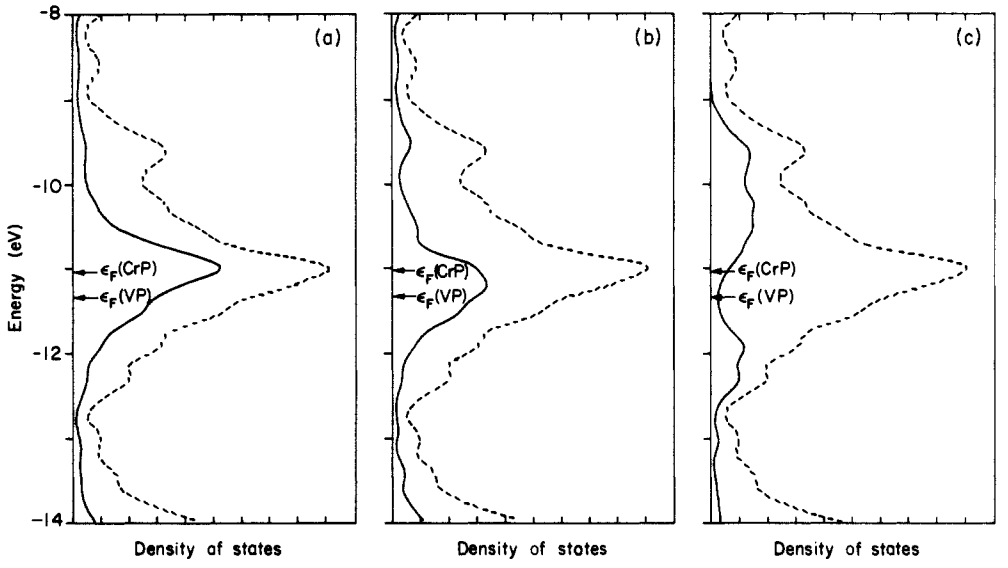

Figure 1. Density of states (DOS) diagrams for the NiAs structure type lattice. The dashed lines give the total DOS, and the dark lines indicate the combinations of (a) x^2-y^2 and xy, (b) xz and yz, and (c) z^2 orbitals of the metal atoms.

Let us compare these expectations to the orbital by orbital contributions to the total density of states (DOS) calculated for MnP in the NiAs structure (Figure 1). Before examining this figure it is useful to recall that in an octahedron with the threefold axis as the z axis of quantization, the t_{2g} and e_g sets are given ideally as linear combinations of xz,yz and x^2-y^2,xy sets, as indicated in **11**.[39] Projecting out the x^2-y^2 and xy, xz and yz, and z^2 orbital contribution to the total DOS in Figure 1 does not quite give the picture that we anticipated in **9** and **10**. Most of the orbitals contribute to one central peak. There is some splitting in case of the z^2 orbitals, and we will see in a moment that this is based on dispersion of bands due to metal–metal bonding. The Fermi level for any electron count between Ti and Co is right within the large peak at ca. −11 eV in the DOS diagram, and we expect these materials to be metallic. This is in accord with the experimental data; most NiAs type materials are metallic.

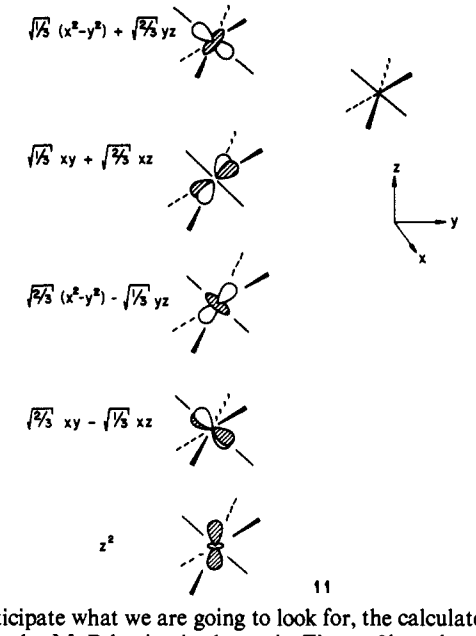

11

To anticipate what we are going to look for, the calculated DOS curve for the MnP lattice is shown in Figure 2b and compared to the DOS curve for the NiAs type structure in Figure 2a. The large peak in the DOS near the Fermi level (ca. −11 eV) is split. At this point one can do some more detective work so as to determine which orbitals contribute most to the bands near the Fermi level. This is done for the xy and y^2 orbitals for both structure types in Figure 2, c and d. The states going down in energy are localized mainly in the plane perpendicular to the hexagonal c-axis. In this plane the new metal–metal bonds are formed.

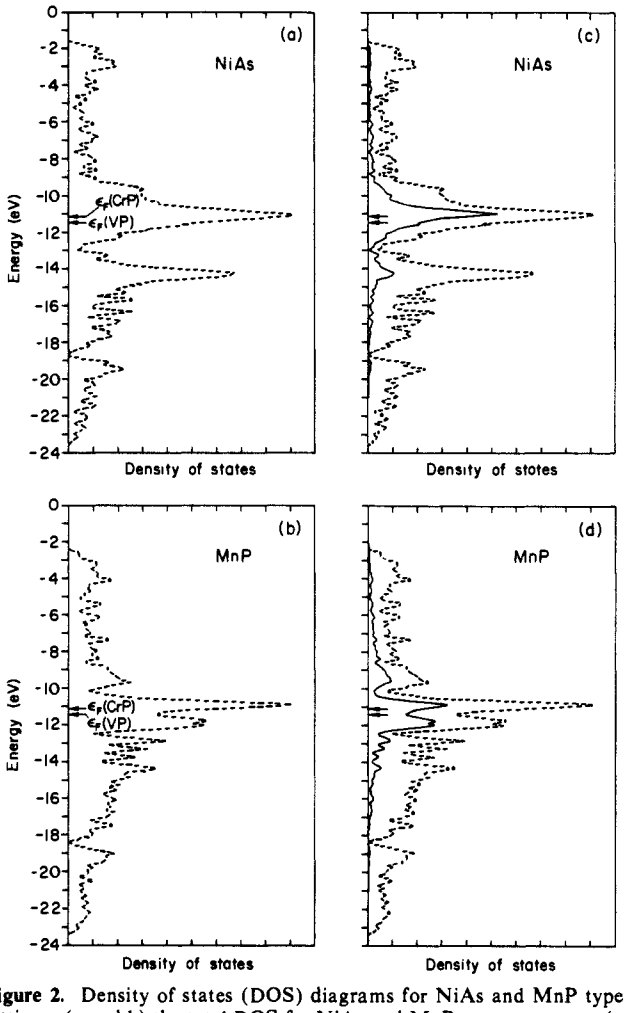

Figure 2. Density of states (DOS) diagrams for NiAs and MnP type lattices: (a and b) the total DOS for NiAs and MnP structure types, (c and d) the combination of the orbitals in the *ab*-plane (dark lines) to the total DOS (dashed lines) in both lattices.

Let us return for the moment to the NiAs lattice. A convenient starting point for building up the band structure for this lattice

(39) (a) Albright, T. A.; Hofmann, P.; Hoffmann, R. *J. Am. Chem. Soc.* **1977**, *99*, 7546. (b) Orgel, L. E. *An Introduction to Transition Metal Chemistry*; Wiley: New York, 1969; p 174.

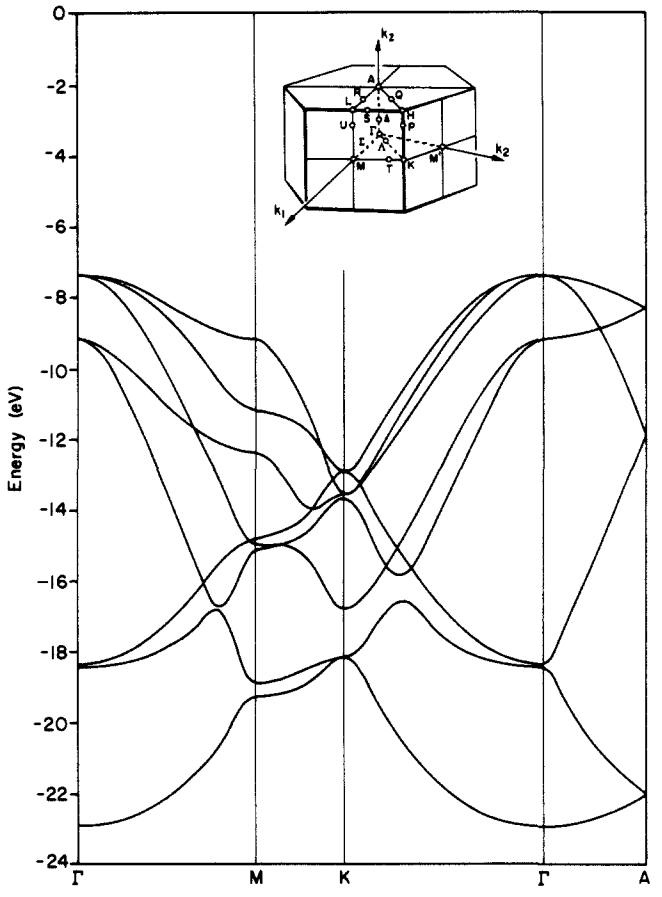

Figure 3. Band structure of a hcp P lattice in 4 directions of the 3-dimensional Brillouin zone.

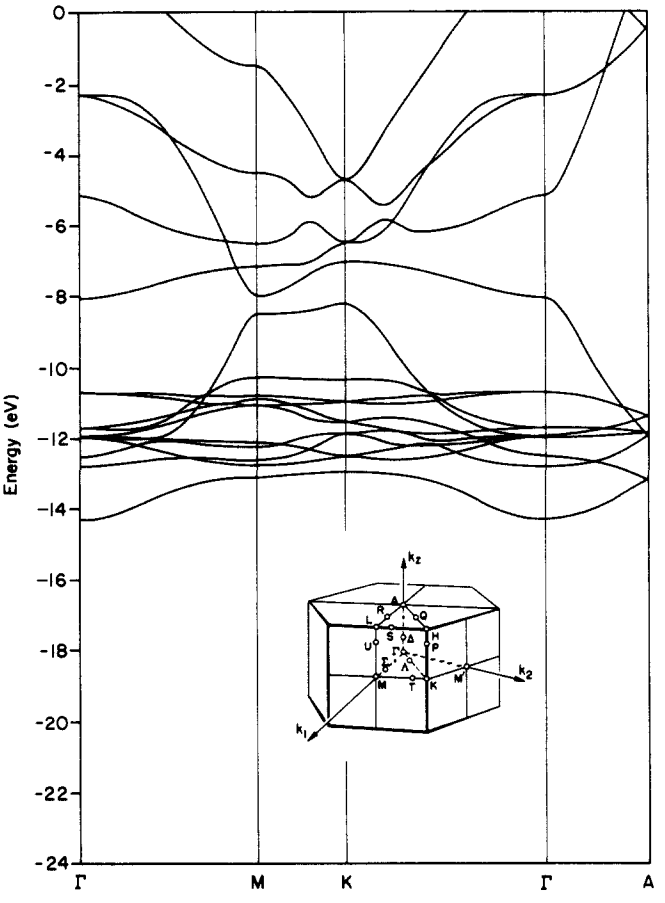

Figure 4. Band structure of a primitive hexagonal Mn lattice in 4 directions of the 3-dimensional Brillouin zone.

is from the phosphorus and manganese sublattices. The P sublattice is hexagonal close packed, and the band structure of a 2-dimensional slab has been described before.[40] We want to repeat here only the essential features of the earlier analysis, those that will help us understand the 3-dimensional case. The unit cell and a representation of the lattice are shown in **12** and **13** and the calculated band structure in Figure 3. At the Γ point we can

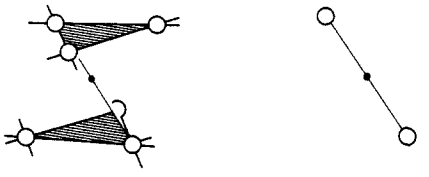

12 13

expect two 3s bands, symmetric and antisymmetric with respect to the inversion center i, lowest in energy. The x,y levels (band 4,5 and 6,7 in Figure 3) **14** and **15** are pushed up in energy because of in-plane interactions. The interplane splitting is small. The

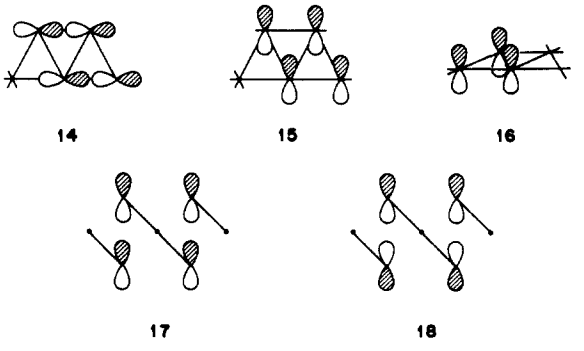

14 15 16

17 18

z orbitals interact weakly in plane **16**, but they are split considerably by interplane interactions (bands 3 and 8 in Figure 3) **17** and **18**. Going from M to K in the hexagonal Brillouin zone, the situation is different. First of all the symmetry is lower and certain degeneracies present at the Γ-point are split. Because we are moving away from Γ, a phase factor is associated with each translation, which makes it difficult to draw out the orbitals. At K, the x,y combination picks up some bonding character and goes down in energy, the interplane interactions still being small. The z orbital develops an appreciable dispersion along Γ–A, due to the large interlayer interaction. Note that there is substantial s–z mixing and that the band dispersion is large even though there is no P···P bonding.

We return for a moment to a point we made earlier: another way to construct the P sublattice is from an AB stacking of triangular (3^6) nets of P atoms, and this construction principle applies to the band structure as well. As the reader may have noticed in the preceding paragraph, we always had a symmetric and antisymmetric combination of bands due to interplane interaction. Let us think for the moment of a simple 2D triangular net of atoms. We have one atom per unit cell and therefore we expect four bands. The s and x,y bands will leave a large dispersion because of σ type in-plane interactions, and the P_z band will be rather flat since the z orbitals are involved only in π interactions. Going next to the hcp lattice we double the unit cell and the number of bands by forming a symmetric and antisymmetric combination. The x,y combination will be split by little, the z combination, however, is split quite a bit due to interplane interactions. This is just the picture we saw in Figure 3.

Next let us look at the Mn sublattice. Here the Mn–Mn interaction is not large, and the splitting of the d band does not exceed 2 eV. The wide 4s band interpenetrates the narrow 3d bands considerably, as can be seen in Figure 4.

Next we turn on Mn–P interactions, combining the two sublattices. The corresponding band structure for the NiAs type

(40) Kertesz, M.; Hoffmann, R. *J. Am. Chem. Soc.* **1984**, *106*, 3453.

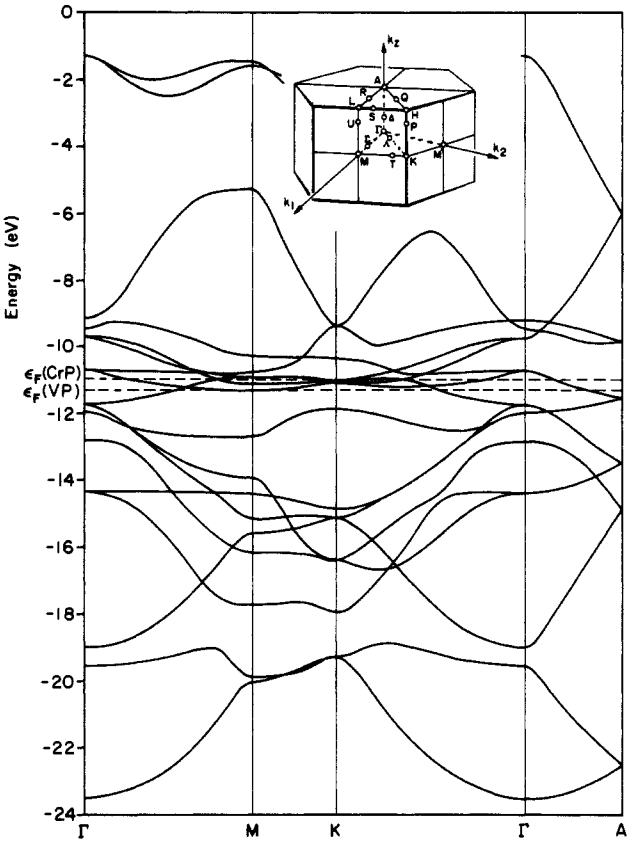

Figure 5. Band structure for a NiAs type lattice along 4 directions of the 3-dimensional Brillouin zone.

lattice is shown in Figure 5. The general shape of the bands is not very different from what we have seen in the partial band structures. Phosphorus bands move down in energy and metal 3d and 4s bands go up in energy, just as expected from a ligand field model. Since the orbitals of the NiAs structure have high symmetry at the Γ point, they are relatively easy to interpret. In the present case, the symmetry at the zone center is $6/mmm$—D_{6h}, the same as the point symmetry of the solid. As soon as we move away from the zone center the symmetry is reduced. Along Γ–M, M–K, and K–Γ it is C_{2v}, along Γ–A C_{6v}. At the Γ point the lowest two bands, a_{1g} and b_{2u} in symmetry, are are phosphorus 3s. The next three bands, 3,4,5 of b_{1g} and e_{2g} symmetry, are phosphorus 3p with significant admixture of metal 3d in the e_{2g} combinations (the other three phosphorus orbitals have been pushed up above the metal d-block by ligand–ligand interactions). Next comes the metal d-block, where the bonding z^2 combination is lowest in energy. It is worth mentioning that bands 9,10 and 11,12 are purely of metal 3d-character without any phosphorus contributions. The reason is a symmetry based one; there is no symmetry-adapted combination of ligand orbitals of appropriate symmetry with which to interact. A similar argument—metal orbitals do not form an e_{1u} combination—applies for bands 13,14. These are the still missing ligand x,y orbitals with some metal 4 p-character mixed in. Band #16 is the out-of-plane combination of the metal z^2 orbitals.

The only symmetry direction along which the bands are relatively easy to interpret is the Γ–A direction, since the structure along that direction bears some resemblance to a chain of face sharing MX_3 octahedra. As pointed out above, the symmetry along the line is C_{6v}, and because of the 6_3-screw axis present all the bands pair up or quadruple at the zone edge. The nondegenerate and degenerate bands can be classified as S,A and e_s,e_A, respectively, which means symmetric or antisymmetric with respect to the 6_3-screw axis, corresponding to in- and out-of-plane combinations of the 3d orbitals. Although one might be tempted to consider the NiAs structure as quasi-one-dimensional in the c-direction, most of the bands along Γ–A are rather flat. However, bands 3 and 6 and 15 and 16, respectively, do not have the same character at the zone center. Technically, the phosphorus z bands 3 and 15 and the metal z^2 bands 6 and 16 should meet at the zone edge. What is happening is an avoided crossing between bands 6 and 15. Another avoided crossing is taking place between bands 4,5 and 14,15.

Now, how are the bands related to the t_{2g} and e_g orbitals of the crystal field picture? The easiest way to see this is at the A-point in the band structure plot in Figure 5. Here the lowest eight bands are mainly ligand in character, the next six correspond to the metal t_{2g} set, and the four highest ones correspond to the e_g orbitals. This nice picture is spoiled when we return to the Γ point. One reason for this is that bands 9,10 and 11,12 do not find a symmetry match among the ligand orbitals and stay "artificially" low in energy. Another reason is that ligand orbitals are pushed up in energy above the metal 3d-block. Looking again at the projections of the DOS in Figure 1, one finds that all metal 3d orbitals except for the z^2 combination are contributing equally to the bunched DOS at the Fermi level. The z^2 combination is split into two peaks (disregarding the "fine structure"). Moreover the COOP curve in Figure 6 shows substantial metal–metal bonding contribution in the c-direction. Does this mean that there is a metal–metal bond?

This question is—as the reader might expect—not new and has been analyzed in detail for a dimer[41] and a one-dimensional chain

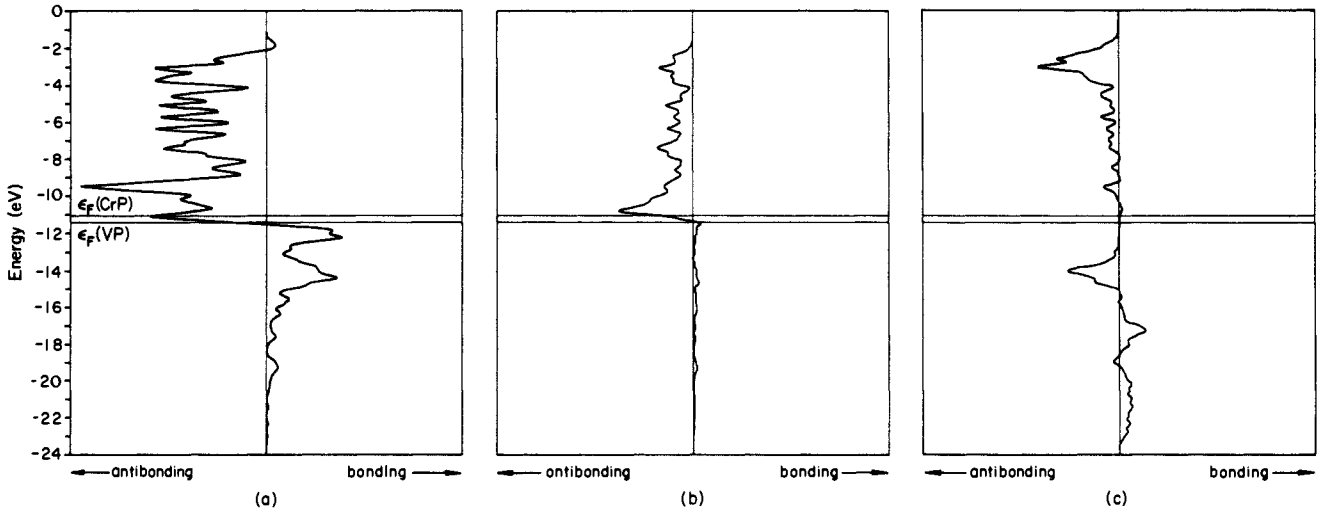

Figure 6. Crystal overlap population (COOP) curves for (a) Mn–Mn contacts parallel to c_{hex} and (b) perpendicular to c_{hex} and (c) for P–P contacts in a NiAs type lattice.

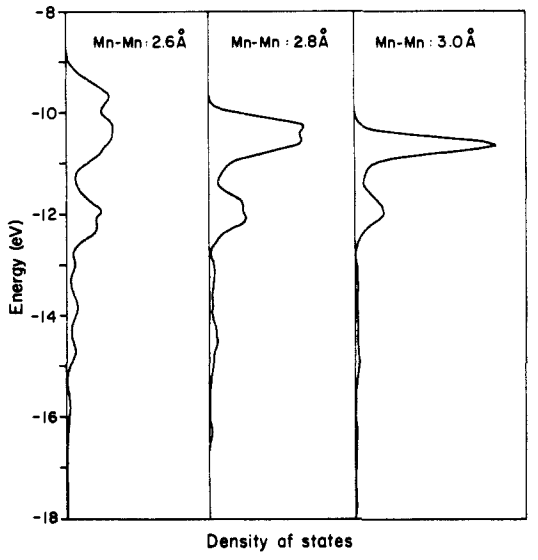

Figure 7. z^2 contribution to the DOS in the NiAs type for 3 different "interlayer" distances.

of face-sharing octahedra[42a] elsewhere. If metal–metal bonds are at all important, the bottom of each band should be metal–metal bonding and the top metal–metal antibonding. Most of the 3d-orbitals, e.g., in band 7,8, are pointing away from the ligands and the chain directions. This results in a narrow band width and a contribution to metal–metal bonding that should be negligible. Only the z^2 orbitals have the proper directionality for bonding.

To get some feeling for the changes that occur in expansion or contraction of the chain, we varied the "interlayer distance" in the NiAs structure from 2.6 to 3.0 Å. The underlying thought was, of course, that in case there is a real metal–metal bond along this direction, the observed splitting for the z^2 orbitals should decrease and the two main peaks in Figure 7 (disregarding the fine structure) should finally collapse. The corresponding DOS projections are shown schematically in Figure 7. Going to larger layer separations, both peaks apparently do not change in energy, but show only some variation in peak height.

We can step back further to understand this behavior and consider the contraction of a one-dimensional model chain of face-sharing MX_3 octahedra. The most severe changes are expected for the metal z^2 orbitals, and so we concentrate only on the $2S^+$, $2S^-$, $3S^+$, and $3S^-$ bands shown for different metal–metal distances in Figure 8. There is clearly a gradual modification of the bands as the chain is contracted. First, at smaller metal–metal distances there is an avoided crossing between the $2S^+$ and $3S^+$ band, indicated in Figure 8 by a dashed line. The $2S^+$ band is mainly phosphorus z, and the $3S^+$ band is metal z^2. The band width of the z^2 band increases on contraction of the chain; however, the $3S^-$ band does not change much in energy. The reason for this behavior is shown in **19**. As the metal–metal

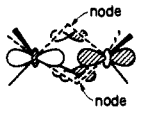

19

distance decreases, the bridging ligands are moving out of the node of the metal fragment. So the increasing metal–metal antibonding interaction is compensated by a gain in through-bond coupling.

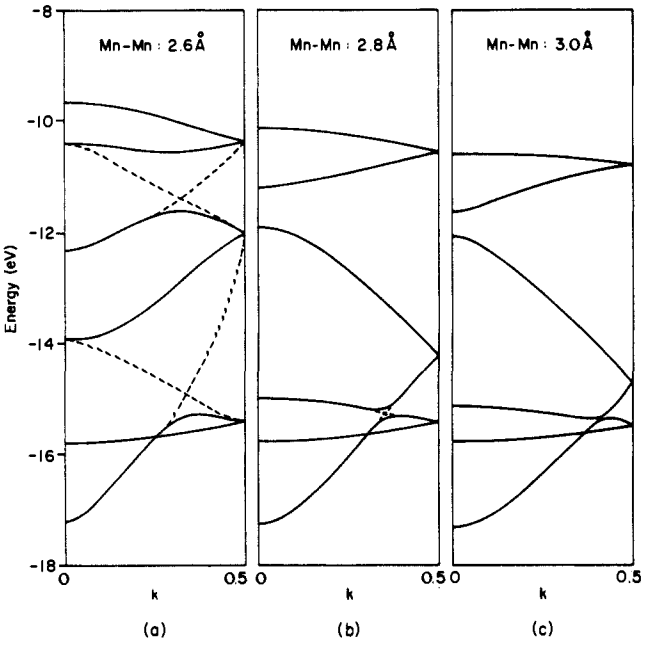

Figure 8. Bands $2S^{(\pm)}$ and $3S^{(\pm)}$ of a 1-dimensional $(MX_3)_\infty$ chain of face-sharing octahedra for 3 different metal–metal distances.

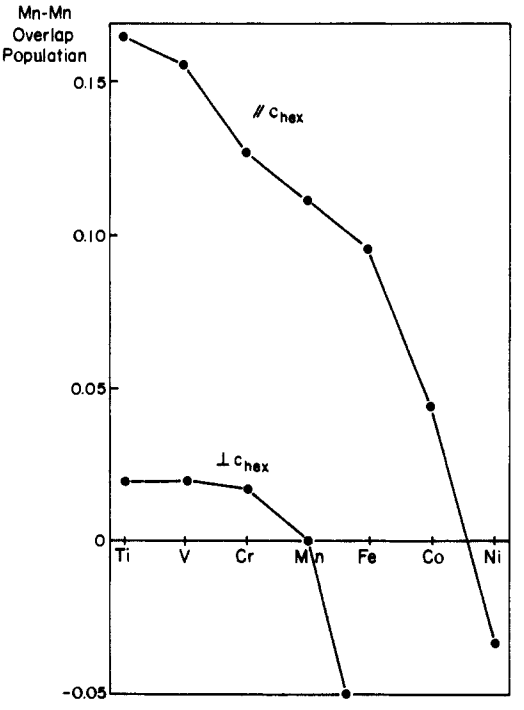

Figure 9. Metal–metal overlap populations as a function of the electron count in the NiAs type lattice: (a) for metal chain parallel to c_{hex} and (b) for metal–metal contacts perpendicular to c_{hex}.

What we observe here is reminiscent of what is described for MS_2 chains elsewhere.[42b] For the $3S^+$ band one has nevertheless the feeling that through space metal–metal interaction is important. Expanding or contracting the MX_3 model chain leads to the same pattern for the z^2 contribution to the DOS, as we have seen in Figure 7 for the variation of the "interlayer distance" in the NiAs type structure.

There is axial metal–metal bonding in the NiAs structure. Figure 9 shows the computed axial and lateral metal–metal overlap populations as a function of electron count. Overlap populations of the order of 0.10 may seem small, but in fact they are substantial, from our experience, and indicative of metal–metal bonding. Note the weak lateral bonding and the fall-off in both with increasing d-electron count, implicit in the COOP curve of Figure 6.

(41) Summerville, R. H.; Hoffmann, R. *J. Am. Chem. Soc.* **1979**, *101*, 3821.

(42) (a) Whangbo, M.-H.; Foshee, M. J.; Hoffmann, R. *Inorg. Chem.* **1980**, *19*, 1723. (b) Silvestre, J.; Hoffmann, R. *Inorg. Chem.* **1985**, *24*, 4108. (c) Yanase, A.; Hasegawa, A. *J. Phys. C: Solid State Phys.* **1980**, *13*, 1989. (d) Perkins, P. G.; Marwaha, A. K.; Stewart, J. J. P. *Theor. Chim. Acta (Berlin)* **1981**, *59*, 569.

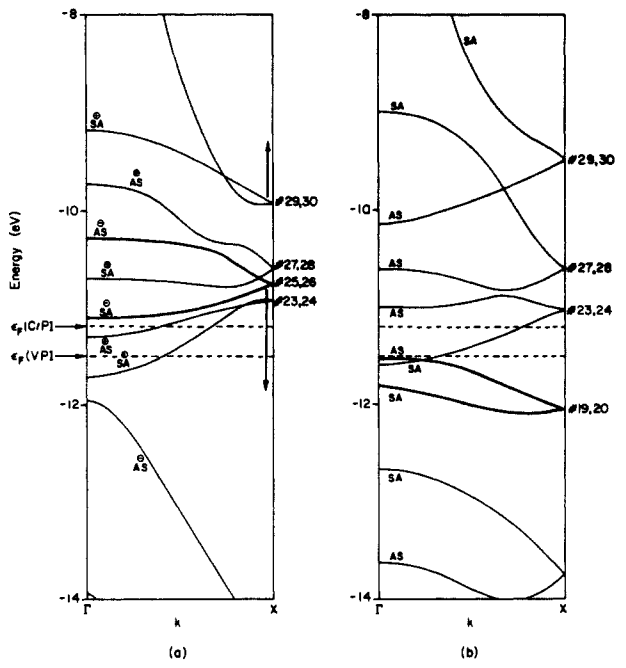

Figure 10. Essential energy bands for the displacive transition from the NiAs (a) to the MnP lattice (b). Heavy lines are the bands driving the distortion.

Many compounds with the NiAs structure exhibit significant magnetic properties. Our one-electron calculations are perforce nonmagnetic, i.e., they cannot allow different spin electrons to move in different orbitals, or, alternatively, to allow different DOS distributions to majority and minority spins. Sometimes the differences in the electron distribution for magnetic and nonmagnetic calculations can be very large indeed—a reviewer directed us to a striking illustration of this in a calculation on MnAs[43a] (see also MnP[43b]). Since our primary interest is in the deformation systematics of these structures, we believe we can nevertheless obtain some guidance from nonmagnetic calculations, but this limitation should be kept in mind.

Distortion to the MnP Structure

We are now prepared to investigate the distortion. As seen in the introduction, the MnP type structure can be viewed as a distorted NiAs structure. The unit cell contains four instead of two formula units. Making full use of the group–subgroup relations in **8**, it is possible (though we will not do so here) to construct the bands of NiAs prepared for the distortion to MnP and then actually carry out the distortion. Our resulting MnP band structure compares well with that given in previous calculations.[43b,c]

Going from the NiAs to the MnP type structure, isolated P–P and Mn–Mn zigzag-chains running in the *a*-direction are formed. Therefore the band structure in the Γ–X direction should be most affected by the distortion. The relevant levels can be labeled along this line according to their symmetry (S) or antisymmetry (A) with respect to operations 2_1 and *n* of space group *Pmcn*. SS and AA bands are not affected much by the distortion. The important bands of SA and AS symmetry, however, change substantially in shape and have been plotted separately in Figure 10, a and b. One pair of bands drops below the Fermi level, indicated by a horizontal arrow on the left side of the figure. Another pair of bands is moving up in energy. This is just the effect we expect to see. Symmetry elements are lost along the line, and some orbitals, of different symmetry in the undistorted structure, now of the same symmetry in the distorted structure, are allowed to mix. As a result, some orbitals are stabilized and some are destabilized. If the orbitals which are stabilized are occupied, we expect the distorted structure to be favored.

These features are reminiscent of a second-order Jahn–Teller effect, with which we are familiar from molecular compounds. The major difference in this case is that mixing occurs along the full symmetry line of the Brillouin zone.

To reveal the essential driving force for the distortion, we concentrate just on the bands drawn in Figure 10, a and b. The symmetry labels in Figure 10, a and b, refer to the twofold screw-axis, and the *n*-glide plane in space group *Pmcn*, the + or − sign in Figure 10a, refers to a twofold axis, which is present in space group *Cmcm* along *a* (zero height in *b* and *c*), but absent in space group *Pmcn*. On going from a to b in Figure 10 the heavy lines, which were either symmetric or antisymmetric with respect to that twofold axis, will mix. This is shown schematically for the X-point, where the orbitals are real, in **20**, **21**, and **22**. Each band is represented at X by a degenerate set of crystal orbitals, which are a linear combination of a σ and π component. The effect of the π-component is only small and can be safely neglected in the sequel. Crystal orbitals of only one metal chain (heavy line

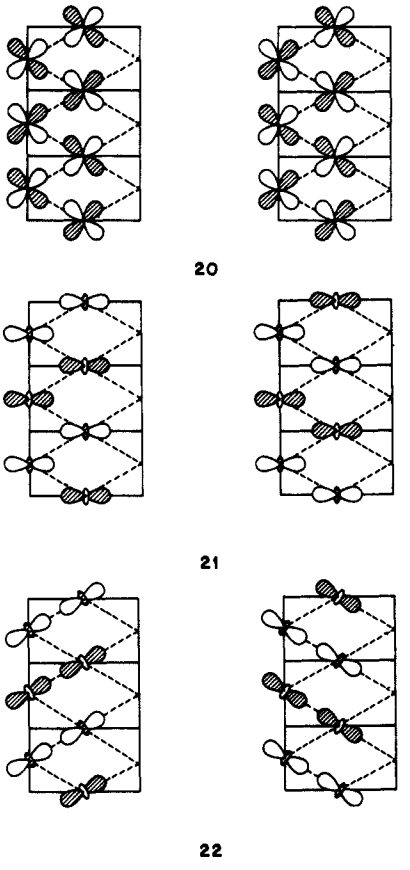

20

21

22

in **5**) are shown, and the other chain is symmetry equivalent. One of the two crystal orbitals, shown in **20**, mainly metal *xy* in character, is strongly bonding within the unit cell and antibonding outside. The opposite is true for the other one. Mixing with crystal orbitals represented in **21**, mainly metal y^2 in character, generates one strongly bonding combination, either within or without the unit cell, as shown in **22**. The lobes causing the antibonding interactions before are now directed into more "innocent" regions of space. In terms of the band structure in Figure 10, a and b, this means that orbitals 25,26 (hexagonal) drop by about 1.2 eV in energy at X, and bands 29,30 pick up antibonding character and are pushed up in energy. The situation at X is, of course, not representative of the unit cell, but it is apparent that metal–metal bonding furnishes substantial stabilization. This shows up in the DOS projections shown above in Figure 2, c and d, where metal *xy* and y^2 contributions were seen to drop in energy for the MnP type structure. The comparison of the COOP curves for the MnP structure given in Figure 11, and for the NiAs structure

(43) (a) Sandratskii, L. M.; Egorov, R. F.; Berdyshev, A. A. *Phys. Status Solidi (b)* **1981**, *103*, 511. (b) Yanase, A.; Hasegawa, A. *J. Phys. C.: Solid State Phys.* **1980**, *13*, 1989. (c) Perkins, P. G.; Marwaha, A. K.; Steward, J. J. P. *Theor. Chim. Acta (Berlin)* **1981**, *59*, 569. (d) Motizuki, K.; Katoh, K.; Yanase, A. *J. Phys. C: Solid State Phys.* **1986**, *19*, 495.

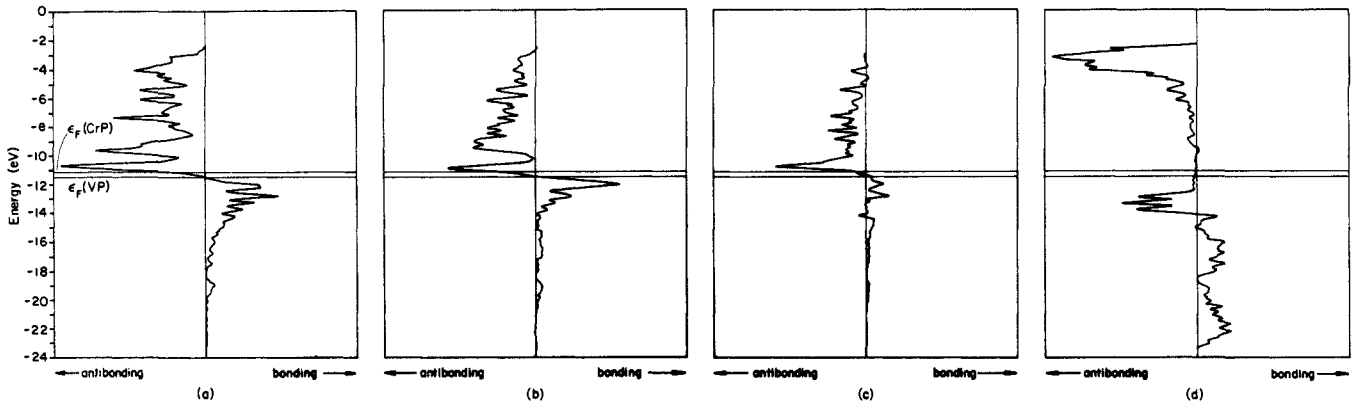

Figure 11. COOP curves for the Mn–Mn contacts (a) parallel to *c*, (b) along the zigzag chain, and (c) along the *a* direction and (d) for the P–P contacts along the P–P chain in the MnP lattice.

type, depicted in Figure 6, is even more instructive, for we see metal–metal bonding developing in the *a,b* plane. The relevant overlap populations in the metal chains rise to 0.10 for a CrP electron count, falling for higher electron counts.

We should once again introduce a cautionary note here that our calculations come from a nonmagnetic calculation. MnP is ferromagnetic, and spin-polarized calculations of its band structure are available.[43b] We still think that insight concerning the factors favoring metal–metal or phosphorus–phosphorus (to be discussed next) bond formation may be gleaned from our simple calculation.

Looking at the P–P overlap population in Figure 13d, one observes an increase of the antibonding character at about −6 eV in the distorted structure. This poses the question whether metal–metal bonding provided by the *xy* and y^2 orbitals is the real driving force for the distortion or rather the formation of P–P bonds. What is behind this question is the fact that metal–metal bonds are presumably weak, whereas any P–P bonds formed are expected to be much stronger. As a consequence of P–P bonding, we should see P–P bonding states going down in energy and P–P antibonding states moving up. Were the Fermi level to fall below the top of the anion bands, this would be a natural way to argue.

One way to approach our question is by examining the atomic charges in both structure types. In case of anion–anion clustering, the structure should contain $[P_n]^{n-}$ units instead of isolated P^{3-} anions and the metal atoms should carry a lower positive charge than in the NiAs structure. Table II, which lists the electron densities for both structure types for different electron counts, shows this not to be true.

One could also look at the phosphorus contribution to the DOS. Around −11 eV, which corresponds to the approximate Fermi level for the electron count in question, about 60% of the P states are below the Fermi level and there are no other P states moving down in energy on distortion. As for the metal atoms, some mixing of phosphorus based orbitals is observed, but these orbitals are occupied in both structural types.

We can actually look at the P–P overlap population in the two structures. In the NiAs structure it is 0.009, and in the chains in the Mn–P structure it is 0.162 for a CrP electron count. This clearly indicates some bonding interaction between the phosphorus atoms. Does this mean that phosphorus–phosphorus bonding is a driving force for the distortion? To be honest we have to admit that we cannot tell with the data at hand. We cannot give any reason why the formation of P–P bonds indicated by the overlap populations does not show up in the electron densities. Perhaps this is a consequence of only weak P–P bonding interactions and we are just at the borderline, where P–P bonds begin to form. For the moment it may be equally well justified to use a picture of P^{3-} anions or $[P_n]^{n-}$ chains, recognizing that the electron counting is a formalism in either case.

We can compare the calculated band structure with a scheme originally proposed by Goodenough.[44] He suggested that the Fermi level is located in a narrow Mn 3d band which is split by the ligand field. In agreement with this the MnP structure commonly occurs in transition-metal compounds existing over a continuous range from $2 \leq n \leq 6$. This picture finds a rough match in our calculated band structure and follows directly from the relationship to the picture we developed for the NiAs structure type.

Table II. Electron Densities in the NiAs and MnP Structure as a Function of the Number of Valence Electrons per Formula Unit

	NiAs		MnP	
electrons	metal	phosphorus	metal	phosphorus
9	4.11	4.89	4.15	4.85
10	5.10	4.90	5.11	4.89
11	6.10	4.90	6.10	4.90
12	7.07	4.93	7.08	4.92
13	8.02	4.98	8.07	4.93
14	8.92	5.08	9.00	5.00

To a first-order approximation certain properties of a solid, such as the specific heat or the magnetic susceptibility which are related to the thermal excitation of electrons, are proportional to the DOS at the Fermi level.[45] Specific heat measurements for MnP[46] revealed that the 3d electrons form fairly narrow bands with a high DOS at the Fermi level. This is also consistent with measurements of the electrical resistivity.[47] From UPS spectra[48] a sharp Fermi edge was found in the MnP 3d band, and there is qualitative agreement of the spectral band shape with the calculated DOS curves.

The MnP–NiP Transition

Going to higher electron counts, e.g., pumping more than six 3d electrons/metal atom into the metal d bands, the MnP structure distorts further. The resulting structure type shown in **9** is the unique NiP structure. This representation emphasizes a "layer like" appearance of the structure as a result of the distortion, the layers of atoms lying parallel to (010) in the setting chosen in **8**. The sheets are stacked in an A···B···A fashion in the [100] direction; each "A-sheet" is connected to the adjacent "B-sheets" via NiP bonds of lengths 2.26 Å. If there were no cation–cation bonds, the P–P pairs would imply divalent Ni and possibly nonmetallic properties. The Ni–Ni contacts, however, which occur in the actual structure, indicate metallic behavior according to the Mooser–Pearson rule.[49,50] The dimerization we observe in

(44) (a) Goodenough, J. B. *J. Appl. Phys.* **1964**, *35*, 1083. (b) See also: Stein, B. F.; Walensky, R. H. *Phys. Rev.* **1966**, *148*, 933.

(45) Kittel, Ch. *Einführung in die Festkörperphysik*; Auflage, Oldenbourg Verlag: München, Wien, 1983; Vol. 6, p 187 and 482.

(46) Takase, A.; Yashima, H.; Kasuya, T. *J. Phys. Soc. Jpn.* **1979**, *47*, 531.

(47) Takase, A.; Kasuya, T. *J. Phys. Soc. Jpn.* **1980**, *48*, 430.

(48) (a) Nakamori, H.; Tsutsumi, K.; Sugiura, C. *J. Appl. Phys.* **1973**, *48*, 430. (b) Gusatinskii, A. N.; Al'perovich, G. I.; Blokhin, M. A.; Minin, V. I.; Finkel'shtein, L. D. *Izv. Akad. Nauk. SSSR, Ser. Fiz.* **1976**, *40*, 2415. (c) Meyers, C. E.; Franzen, H. F.; Anderegg, J. W. *Inorg. Chem.* **1985**, *24*, 1822. (d) Domashevskaya, E. P.; Terekhov, V. A.; Ugai, Ya. A.; Nefedov, V. I.; Sergushin, N. P.; Firsov, M. N. *J. Electron Spectrosc. Relat. Phenom.* **1979**, *16*, 441. (e) Kakizaki, A.; Sugawana, H.; Nagakura, I.; Ishii, T. *J. Phys. Soc. Jpn.* **1980**, *49*, 2183.

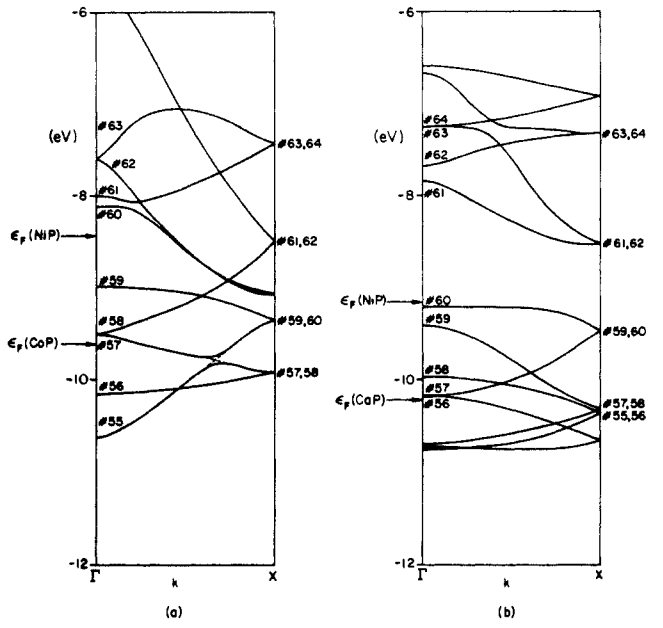

Figure 12. Essential energy bands along the Γ–X line for the distortion from the MnP to the NiP type lattice: (a) MnP structure and (b) NiP structure.

this structure, accompanied by rupture of the phosphorus and metal chains present in the MnP structure, is what we want to examine in the last part of this paper.

The band structure of the undistorted NiP structure can be generated without doing any further calculations from the MnP band structure by a folding back process. Going from one to the other structure the unit cell has to be doubled along the *a* direction. The new Brillouin zone is only half as big as the old one, and all the bands can be mapped into the smaller Brillouin zone. The result is shown in Figure 12a. The electron count for NiP is 120 electrons/unit cell, and we see immediately some steep bands around the Fermi level, indicated again by an arrow in Figure 12a. The bands are partly filled, and the introduction of an energy gap induced by a structural deformation should stabilize the occupied levels in the vicinity of the Fermi level. What should happen is analogous to a pairing distortion, shown in **23**, for a linear chain of hydrogen atoms distorting to diatomic molecules.

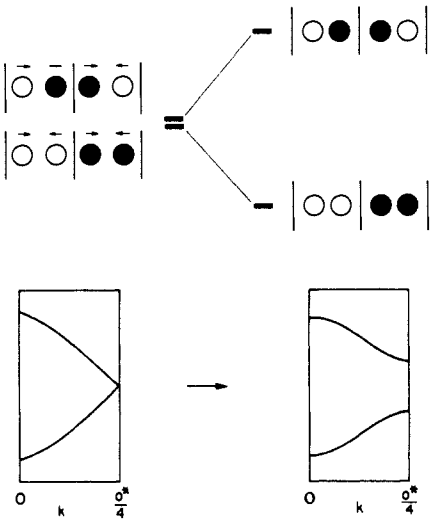

23

The essential part of the band structure for the experimental NiP structure is shown in Figure 12b along the Γ–X direction. Note again that in order to be consistent with the coordinate system chosen in the previous cases, we are using a setting different from the standard choice of axes for the NiP structure. The picture we see in Figure 12b is quite different from the schematic drawing in **23**. The reason for this lies—as we can guess already from the symmetry assignment of the bands—in the twofold screw axis or in more general terms a nonsymmorphic symmetry element along the symmetry line Γ–X. If we recall for a moment the NiP structure in **8**, we recognize that this is a consequence of atoms 1 and 6 or 2 and 5 switching places in the projection given, as pointed out before. Not because we have a pairing of metal and nonmetal atoms, but due to the doubling of the unit cell, atoms 6 and 7 (instead of 6 and 2) are related by a twofold screw axis, and although the screw axis, originally relating atoms 3 and 4 or 1 and 2 in the MnP type structure, is lost, all the bands have to find another partner at the zone boundary. The net effect is—just as shown in **23**—the introduction of an energy gap in the Γ–X direction.

The following discussion is for reasons of clarity confined to only two bands. The dominant driving force for the distortion is the splitting of the degenerate pair 62/63 at the zone center in Figure 12a. We show in **24** and **25** the crystal orbitals of this pair, again for only one layer of metal atoms (the other one is

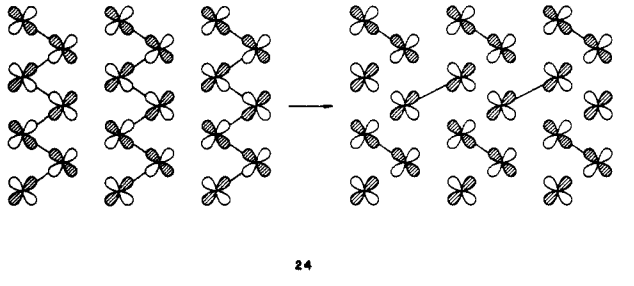

24

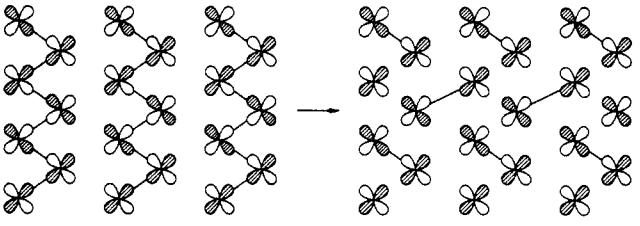

25

related by a glide plane). The phosphorus contribution is shown separately in **26** and **27**. Making the distortion stabilizes **24** substantially; bonding interactions are reenforced, and antibonding interactions are relieved. The antibonding combination in **25** will

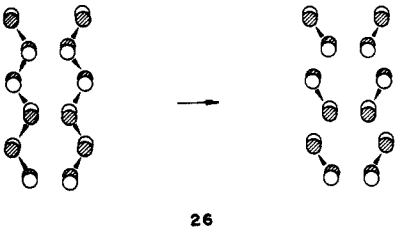

26

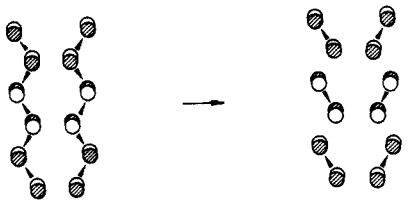

27

(49) (a) Mooser, E.; Pearson, W. B. *Phys. Rev.* **1956**, *101*, 1608. (b) *J. Electron.* **1956**, *1*, 629. (c) Prog. *Semicond.* **1960**, *5*, 103.
(50) (a) Hulliger, F.; Mooser, E. *J. Phys. Chem. Solids* **1963**, *24*, 283. (b) *Prog. Solid State Chem.* **1965**, *2*, 330.

be pushed up high in energy. What happened to the metal part of the crystal orbital in **24** and **25** applies to the phosphorus part in **26** and **27** as well. **26** is stabilized significantly, and **27** will be pushed up. The result is an energy gain of about 2 eV due to this crystal orbital at the zone center. The essential part of the crystal orbital 61, 62 at the zone edge for the undistorted structure is depicted in **28** and **29** (only the metal d_{xy} contribution is shown here). Again we see that one partner of this combination is pushed up and the other one is slightly stabilized. As a consequence, the degenerate pair is split and an energy gap opens up.

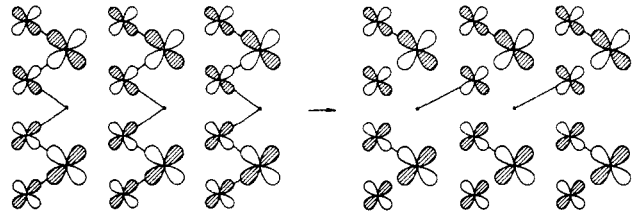

28

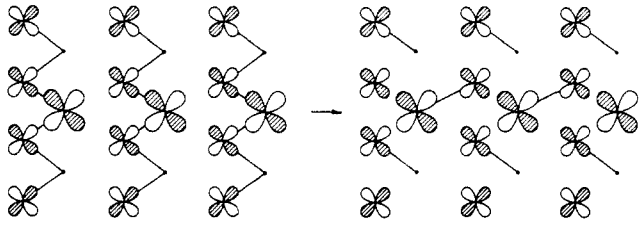

29

One other notable feature of the MnP–NiP distortion is that phosphorus orbitals are involved. As in the NiAs–MnP case, one might ask whether metal–metal bonding is the driving force of the distortion. To answer this question a look at the DOS and COOP curves in Figures 13 and 14 may be helpful. Some metal–metal bonding interactions are lost on going from the MnP to the NiP type structure in the energy range between −8 and −10 eV, as can be gleaned from a comparison of Figure 14b and Figure 11b. Around the Fermi level we do not see a substantial change in P–P bonding, but from the DOS integration and the COOP curve we recognize that antibonding phosphorus states have moved up in energy, compared to the MnP type structure. This is in accord with the simple picture that antibonding states are pushed up higher in energy when a bond is strengthened. When one of our earlier arguments is again used, the formation of P_2^{4-} pairs in the NiP structure could be expected to show up in a more negative charge on the phosphorus atoms, compared to the MnP-structure type, where $[P_n]^{n-}$ chains are present. Looking at electron counts of ≈15–16/formula unit, this is in fact what we see. It must be admitted, however, that this is a little bit of circular reasoning, because a higher charge on the phosphorus atoms is just the result of higher phosphorus contribution to the wave function. Nevertheless, both phosphorus–phosphorus *and* metal–metal interaction seem to be responsible for the distortion.

Since most of the metal d-bands are filled at the Fermi level there is not much metal–metal bonding left. The main metal–metal interaction is, as we can judge by a look at Figure 14a,b, along the metal chain in the (001) projection direction. Although from the plotted band structure along Γ–X in Figure 12b NiP seems to be semiconducting, it is predicted to be overall metallic from the total DOS curve in Figure 13. The physical properties of the real material are not well established, but NiP is reported to be metallic and to become superconducting at ≈1.4 K.[51]

The last point to be mentioned is the energetics of the observed deformations. In order to compare all three structures, we used a rigid band model with parameters for Mn and P. For the

(51) Alekseevskii, N. E.; Mikhailov, N. N. *Soviet Phys. JETP* **1963**, *16*, 1493.

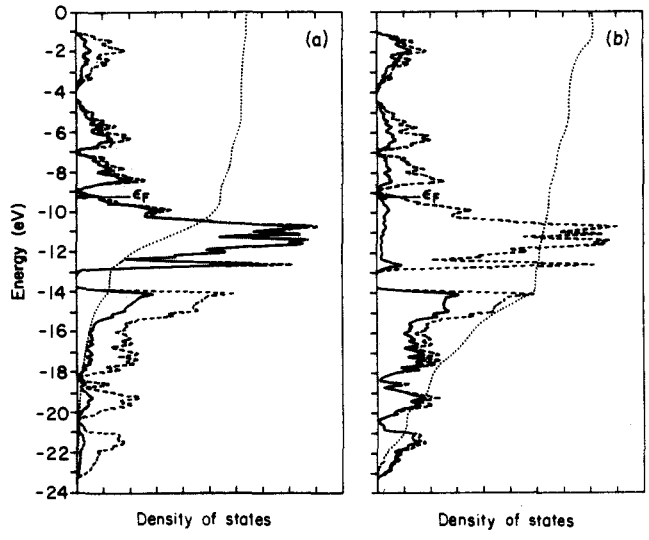

Figure 13. Contributions of (a) metal and (b) phosphorus orbitals to the total DOS for the NiP lattice. The dashed line is the total density of states, and the dotted line is the integration curve. The Fermi level for NiP is marked by an arrow.

geometry in the NiAs–MnP transformation we had the choice between two situations: (i) starting from the experimental MnP structure take the average MnP distance for the (hypothetical) NiAs structure—this implies by itself longer metal–metal distances; or (ii) keep the metal–metal distances similar, which means a shorter MnP distance in the NiAs type structure. In practice we used the experimental geometry for MnP and calculated the total energies for both extremes. From what we said it is already apparent that the energy calculations are troublesome, because no matter what we did the MnP distances could never be kept constant.

Total energies in Figure 15 were obtained for both of the above possibilities. Energies were calculated for electron counts from d^1 (TiP) to d^7 (NiP) and are plotted with the energies of the NiAs structure as the reference zero line in Figure 15. This means above the abcissa the NiAs structure is more stable and below the abcissa the MnP structure. Our calculations always render the NiAs structure type more stable. This is not true, and the reason for this discrepancy is probably the change in the MnP bond distances. Also it will be recalled that our calculations cannot treat the magnetism of these structures, and the consequent effect on energies, properly. Since we know that we have difficulties in getting absolute energy values right, we just look at the shape of the energy difference curve. Both curves show an approximate U shape: for smaller and higher electron counts the NiAs structure is more stable, for intermediate electron counts the MnP structure is preferred. Shifting the baseline by about 4 eV to the dashed line in Figure 15, e.g., assuming that we are 4 eV off in the energy values, gives us for curve *a* a good agreement with experiment; for electron counts up to d^2 we have the NiAs structure more stable, between d^3 and d^6 the MnP structure, for d^7 the NiAs structure. Starting from the d^7 electron count, however, the NiP structure is according to graph c in Figure 15 lowest in energy. This is also in agreement with the experimental facts.

Summary and Concluding Remarks

In this contribution we have tried to shed light on structural deformations observed among simple transition-metal phosphides. Starting from the high-symmetry NiAs type structure we followed a sequence of structural deformations with increasing electron count. For d^1 and d^2 systems the NiAs structure type is preferred, and for d^3 and d^6 systems a distortion to the MnP type structure occurs. We constructed the band structure of the NiAs structure in detail and discussed the importance of direct and indirect metal–metal bonding. The NiAs–MnP distortion is found to result from a second-order Jahn–Teller type distortion, splitting a peak in the density of states of the NiAs type structure. The stabilization is due to an increased metal–metal interaction in the

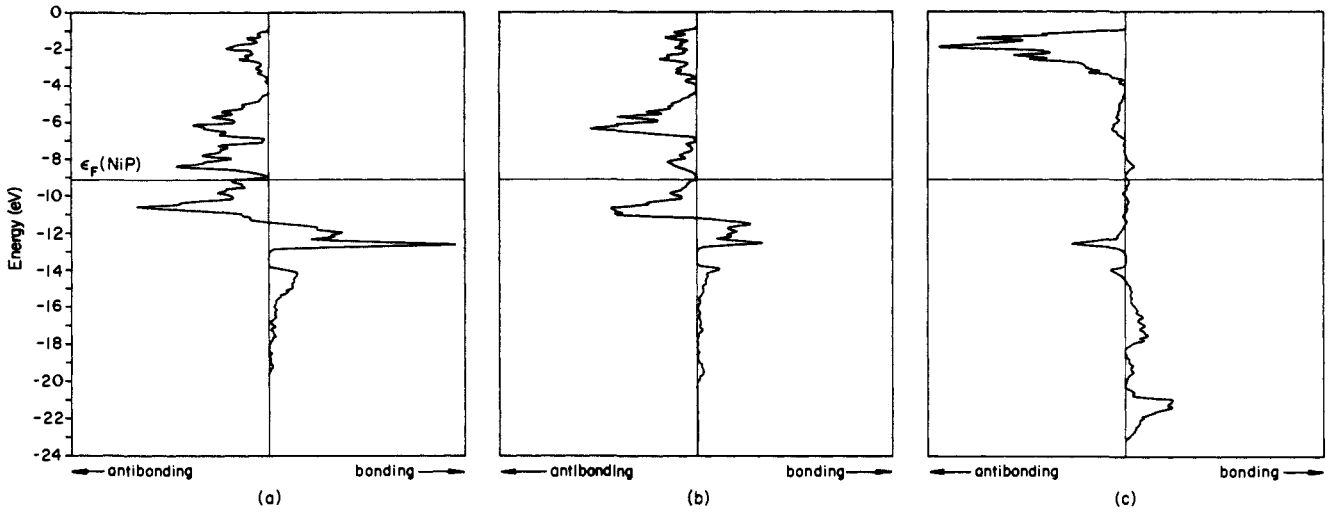

Figure 14. COOP curve for metal–metal contacts (a) parallel to c, (b) perpendicular to c, and (c) for P–P bonding in the NiP structure.

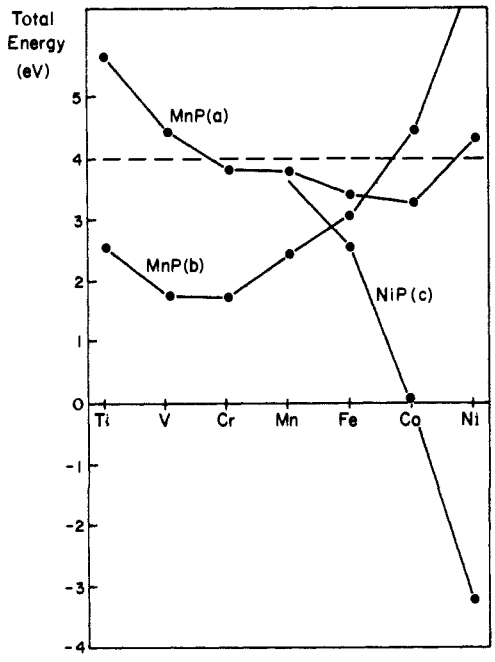

Figure 15. Total energy curves for the MnP (a, b) and NiP (c) lattice relative to NiAs structure as zero. For obtaining curve a metal–metal distances and for curve b metal–ligand distances were kept constant.

distorted structure. In the analysis of the distortion, the use of minimal group–subgroup relationships for the structures proved to be very useful. Bonding interactions between pairs of metal *and* phosphorus atoms are responsible for the distortion from the MnP to the NiP structure type. This introduces an energy gap in the density of states in the symmetry direction where the distortion occurs.

The deformation to the MnP structure is very general in type and may be regarded as one of the *prototypical distortions of a triangular* (3^6) *net of atoms*. A similar distortion mechanism can be expected in CdI_2 type phases. $NbTe_2$ and $TaTe_2$ for instance distort on cooling from a high-temperature CdI_2 to a monoclinic structure[52] with metal zigzag chains.[15,29,53] It may be interesting to remark that the same relationship as between the NiAs and MnP structure types exists between the Ni_2In (filled NiAs type) and the Co_2Si type.[54-56] Transitions between these structure types

Table III. Extended Hückel Parameters

orbital		H_{ii}, eV	ζ_1[a]	ζ_2	c_1[a]	c_2
Mn	3d	−11.67	5.15	1.7	0.5140	0.6930
	4s	−9.75	1.8			
	4p	−5.89	1.8			
P	3s	−18.6	1.8			
	3p	−14.0	1.8			

[a] Exponents and coefficients in a double $-\zeta$ expansion of the 3d orbital.

are reported, for instance (second order) phase transitions for Ni_2Si,[57] MnCoGe or MnNiGe,[56b,c] and TiNiSi or $TiCoSi$[56b] as a function of temperature and for $Pd_{2-x}Sn$[58] as a function of composition. According to Aizu[15d] their space groups ($P6_3/mmc$ for Ni_2In and *Pnma* for Co_2Si) are connected by a ferroelastic transformation, or in a different notation, there is a group–subgroup relation as required by Landau's rules.[15] The corresponding symmetry reduction causes some bands to mix in a manner related to that discussed in the NiAs–MnP case. Similar reasoning can be applied in cases where the nonmetal atoms are arranged in more complicated stacking sequences, as found in the Nb_2Se_3[31] and Nb_3Se_4[34] types.

Acknowledgment. W.T. especially thanks Ralph Wheeler and Chong Zheng for sharing their expertise with him and Professor A. Simon for some enlightening discussions. His stay at Cornell was supported by a fellowship from DAAD/NATO. Our research at Cornell was generously supported by the National Science Foundation through Research Grant DMR 8217227A02 to the Materials Science Center. We are grateful to Cora Eckenroth for the typing and Jane Jorgensen and Elisabeth Fields for the drawings.

Appendix I

The extended Hückel method[36,37] in the tight-binding approximation[38] was used in all calculations. All parameters listed in Table III were taken from previous work.[60] Experimental geometries were used for MnP[9] and NiP.[18] The geometry in the NiAs type structure was either generted from the condition a(hex) = a(orth) and c(hex) = 1.633a(hex) or from an MnP distance of 2.358 Å, obtained as an average MnP distance from the

(52) Van Landuyt, J.; Van Tendeloo, G.; Amelinckx, S. *Phys. Stat. Solidi* **1975**, *A29*, K11.
(53) Brown, B. E. *Acta Crystallogr.* **1966**, *20*, 264.
(54) Jellinek, F. *Z. Österr. Chem.* **1959**, *60*, 311.
(55) Aroussen, B.; Lundstrom, T.; Rundqvist, S. *Silicides, Borides* and *Phosphides*; Methuen and Co.: London, 1965; p 69.
(56) (a) Johnson, V.; Jeitschko, W. *J. Solid State Chem.* **1972**, *4*, 123. (b) Johnson, V. *Inorg. Chem.* **1975**, *14*, 1117. (c) Jeitschko, W. *Acta Crystallogr.* **1975**, *B31*, 1187.
(57) Toman, K. *Acta Crystallogr.* **1952**, *5*, 329.
(58) Schubert, K.; Lukas, H. L.; Meissner, H. G.; Bhan, S. *Z. Metallkd.* **1959**, *50*, 534.
(59) Hizer, K. *J. Phys. Soc. Jpn.* **1969**, *27*, 387.
(60) Hoffmann, R.; Zheng, C. *J. Phys. Chem.* **1985**, *89*, 4175.

MnP-type structure and the ideal axial ratio of 1.633.

A 28k-point set for the hexagonal structure and a 27k-point set for the orthorhombic phases were used in the irreducible wedge[61] of the Brillouin zone for the density of states calculations.

Appendix II

The symmetry relation between crystal structures can be made more transparent by the use of maximal subgroup–minimal supergroup relations.[12-14] The maximal nonisomorphic subgroups U of a space group G are divided into two types: (I) t = "translationsgleich" (lattice-equivalent) and (II) k = "klassengleich" (class equivalent). In case I the subgroup U contains all translations of G and its crystal class is of lower symmetry than that of G. In case II G and U have the same crystal class but belong to different space group types. Thus U has lost translational symmetry, i.e., the primitive cell of U is larger than that of G. The index of a subgroup U (i.e., t3 or k2) is the number of cosets of U in G. The general formulation of the symmetry relations is given in the form

Hermann-Mauguin symbol of G

↓ type and index of U
↓ unit cell transformation
↓ origin shift

Hermann-Mauguin symbol of U

(61) Pack, J. D.; Monkhorst, J. J. *Phys. Rev.* **1977**, *B16*, 1748.

Electrochemical Evidence for a Three-Center, Three-Electron Agostic Interaction in Tungstenocene Dialkyl Cations and Estimation of the Magnitude of the Interaction

Marianne F. Asaro, Stephen R. Cooper, and N. John Cooper*

Contribution from the Department of Chemistry, Harvard University, Cambridge, Massachusetts 02138. *Received August 26, 1985*

Abstract: The role of three-electron agostic interactions in the chemistry of d^1 tungstenocene alkyl complexes has been explored electrochemically. Cyclic voltammograms in acetonitrile of the dialkyls $[W(\eta\text{-}C_5H_5)_2RR']$ (R = R′ = CH_3, CH_2CH_3, or $CH_2C(CH_3)_3$; R = CH_3, R′ = CH_2CH_3, $CH(CH_3)_2$, or Ph; R = CH_2CH_3, R′ = CH_2Ph), of the alkyl and aryl halides $[W(\eta\text{-}C_5H_5)_2RX]$ (R = CH_3, X = Cl or I; R = CH_2CH_3, X = Cl or I; R = $CH(CH_3)_2$, X = Cl; R = $CH_2C(CH_3)_3$, X = Cl; R = Ph, X = Cl, Br, or I), and of $[W(\eta\text{-}C_5H_5)_2(CH_3)(OCH_3)]$ exhibit a reversible one-electron oxidation between −450 and +125 mV vs. SCE. The substituent effects are additive and result from a combination of inductive effects and π-effects involving donation into the partially occupied frontier orbital of the metal. Methoxide is the strongest π-donor, and only $[W(\eta\text{-}C_5H_5)_2(CH_3)(OCH_3)]$ has a low potential, reversible second oxidation. The donor interactions of the halides (Cl > Br > I) reverse the usual electronegativity trend, probably because of unusually good d–p π-overlap. The π-donor effects of the alkyl ligands suggest a stabilizing three-electron agostic interaction in the cations, controlled by steric repulsion between the alkyls and the cyclopentadienyl ligands. Partitioning the substituent effects in branched alkyls into inductive and agostic components suggests that agostic interactions with methyl and ethyl ligands stabilize the d^1 metal center by up to 2.7 and 0.7 kcal mol^{-1}, respectively.

We have recently demonstrated that hydrogen atom abstraction from the paramagnetic tungstenocene dialkyl cations $[W(\eta\text{-}C_5H_5)_2RR']^+$ (R = R′ = CH_3 or CH_2CH_3; R = CH_3, R′ = CH_2CH_3) is an α-selective process, giving rise to highly reactive intermediate cationic alkylidene complexes.[1] We have also speculated that this α-selectivity reflects ground-state delocalization of unpaired electron density from the metal center on to an α-C–H bond, possibly via overlap of the α-C–H bond with the half-filled frontier orbital of the 17-electron bent metallocene moiety;[1b-d] such a three-center, three-electron interaction is reminiscent of the three-center, two-electron interactions involving overlap of vacant transition-metal orbitals with α- or β-C–H bonds for which the term agostic was recently coined.[2]

Agostic interactions can significantly stabilize diamagnetic, electronically unsaturated complexes, and the importance of such interactions in the reaction chemistry of transition-metal alkyls has been underlined by two recent reports of "alkene hydrides" with β-agostic ground states[3] and by the observation that β-agostic interactions may play a crucial role in Ziegler–Natta polymerization of alkenes by stabilizing the coordinatively unsaturated alkyl intermediates.[4] The only fully established example of an analogous three-center, three-electron interaction in a paramagnetic transition-metal complex, however, is in an early structural study[5] which established that the interaction between an allylic C–H bond and the metal in the 16-electron cyclooctenyl cation $[Fe(\eta^3\text{-}C_8H_{13})\{P(OMe)_3\}_3]^+$ was partially retained in the neutral 17-electron complex $[Fe(\eta^3\text{-}C_8H_{13})\{P(OMe)_3\}_3]$.

Since the paramagnetic tungstenocene dialkyl cations may provide unusual examples of three-electron agostic interactions and since such interactions may also play a significant role in the chemistry of the complexes, we have investigated the cations by using the physical techniques previously reported to provide evidence for agostic interactions.[2] We have been unable so far, however, to structually characterize any of the cations,[6] the

* Fellow of the Alfred P. Sloan Foundation, 1982–1985.

(1) (a) Hayes, J. C.; Pearson, G. D. N.; Cooper, N. J. *J. Am. Chem. Soc.* **1981**, *103*, 4648. (b) Hayes, J. C.; Cooper, N. J. *J. Am. Chem. Soc.* **1982**, *104*, 5570. (c) Hayes, J. C.; Cooper, N. J. *Organometallic Compounds: Synthesis, Structure, and Theory*; Texas A & M University Press: College Station, 1983; p 353. (d) Hayes, J. C.; Jernakoff, P.; Miller, G. A.; Cooper, N. J. *Pure Appl. Chem.* **1984**, *56*, 25.

(2) Brookhart, M.; Green, M. L. H. *J. Organomet. Chem.* **1983**, *250*, 395.

(3) (a) Brookhart, M.; Green, M. L. H.; Pardy, R. B. A. *J. Chem. Soc., Chem. Commun.* **1983**, 691. (b) Cracknell, R. B.; Orpen, A. G.; Spencer, J. L. *J. Chem. Soc., Chem. Commun.* **1984**, 326.

(4) Schmidt, G. F.; Brookhart, M. *J. Am. Chem. Soc.* **1985**, *107*, 1443.

(5) Harlow, R. L.; McKinney, R. J.; Ittel, S. D. *J. Am. Chem. Soc.* **1979**, *101*, 7496.

0002-7863/86/1508-5187$01.50/0 © 1986 American Chemical Society